Coordination Chemistry Reviews, 88 (1988) 69–131
Elsevier Science Publishers B.V., Amsterdam – Printed in The Netherlands

OPTICAL SPECTROSCOPY OF EXCHANGE-COUPLED TRANSITION METAL COMPLEXES

PAUL J. McCARTHY

Department of Chemistry, Canisius College, Buffalo, NY 14208 (U.S.A.)

HANS U. GÜDEL

Institut für anorganische Chemie, Universität Bern, Freiestrasse 3, CH-3000 Bern 9 (Switzerland)

(Received 27 August 1987)

CONTENTS

0010-8545/88/$22.05

A. INTRODUCTION

Exchange-coupled insulating coordination compounds have been the subject of many reports during the past decades by both physicists and chemists. Since the essential phenomenon involves pairing of electron spins, it is not surprising that magnetic susceptibility measurements, magnetic neutron scattering and electron spin resonance (ESR) spectroscopy have been the principal experimental methods used. Optical absorption and emission spectroscopy can be used as complementary techniques, but they can in many cases also offer unique information not available from these other techniques.

In this article we will review the optical spectroscopy of exchange-coupled clusters (largely dimers) of transition metal ions. Discrete polycentered molecules containing two or more magnetic metal ions connected by bridging groups will be discussed, as well as clusters formed by doping a paramagnetic metal into a host lattice. In the latter case, when doping is light, the clusters will be limited mainly to two or three members. We will not treat the exchange interactions in extended magnetic lattices such as pure Cr_2O_3, but we will treat doped systems such as Cr^{3+} in Al_2O_3. In general, we omit treatment of systems which contain direct metal–metal bonding, i.e. we restrict the discussion to systems in which the interionic interactions are much smaller than intraionic effects, such as ligand-field and electron-repulsion interactions.

In order to keep the article both unified and of reasonable length, we will limit the topic as follows. (a) Only optical, i.e. electronic, spectra will be treated; other spectra (IR, Raman, ESR etc.) will be referred to when they offer important confirmatory or supplementary information. (b) Only the spectra of exchange-coupled systems will be treated. Single-ion spectra will be mentioned only where needed to clarify those of the clusters. (c) Only spectra of species in the solid state (crystals and polycrystalline materials) will be discussed, and the emphasis is on measurements on these materials at low temperature.

In Section B the general spectroscopic phenomena of exchange coupling are discussed, mostly in the form of representative examples. A minimum of theory is presented, so that the basic effects can be understood. In Section C we discuss in some detail the spectroscopic techniques used in studying exchange-coupled systems. We include modern techniques which are not yet

routinely used by chemists, but which have been employed by physicists in related areas. Liberal use is made of examples from the recent literature. In Section D we summarize research on the principal types of complexes that have been studied. In this latter section some reports are discussed in detail and others only briefly. The literature coverage is extensive, but not exhaustive. We consider, however, that no significant aspect of the subject has been overlooked.

B. EXCHANGE EFFECTS IN OPTICAL SPECTRA

(i) Energy splittings

(a) Effects which contribute to spectral splittings

The well-known Tanabe–Sugano diagrams show the energy levels arising from the action of a cubic ligand field on the d orbitals of a metal. The transition to a given excited state, expected from the diagram to be a single sharp transition, is rarely found to be such. The band may be broadened and/or split into several components. The principal broadening effect for spin-allowed d–d bands lies in the fact that they are due to $t_2 \rightarrow e$ electron promotions. This leads to different equilibrium geometries in the ground and excited states along the totally symmetric normal coordinate. Such bands thus involve a progression, usually unresolved, in the totally symmetric vibrational mode. In this progression the intensity distribution will follow the Franck–Condon factors. Such bands are usually not informative as far as electronic splittings are concerned. Examples of spin-allowed transitions are the double excitations discussed in Section B (iv) of this review.

Spin-forbidden excitations within the ground state electron configuration are much more informative. They consist of sharp lines with most of the intensity located in the origins. Such intraconfigurational or spin-flip excitations are the principal objects of investigation when exchange effects are studied by optical spectroscopy, but even these spin-forbidden transitions may contain a number of components, since the electronic states can be split into a number of levels by several mechanisms. If, for example, the symmetry is lower than cubic, orbitally degenerate E and T states may be subject to splitting into two (E and T states) or three (T states) orbital components. Likewise, if the electronic state has spin and/or orbital degeneracy, the coupling of the spin and orbital angular momenta (spin–orbit coupling) may lead to measurable splittings. Both the ground and the excited state(s) can further couple with molecular or lattice vibrations (vibronic coupling) to yield a series of vibronic levels. Finally, in polynuclear systems, exchange interactions in both ground and excited states can lead to energy splittings. While the effects of each of these four factors can be observed in the spectra

of complexes, it is the last factor that we wish now to consider in some detail.

Exchange interactions are those which have their origin in the electrostatic forces experienced by the unpaired electrons on neighboring magnetic ions. They are often called magnetic interactions, since magnetic phenomena such as ferromagnetism and antiferromagnetism have their origin in these interactions. Formally, exchange interactions are treated as spin–spin interactions (cf. Section B (i) (c), but it is important to realize that their physical origin is electrostatic.

(b) Experimental manifestation of exchange effects

At the start, we might ask what are the principal effects of exchange coupling that can be observed in optical spectroscopy. They can be summarized as follows.

(1) Spin-allowed d–d bands are basically unaffected by exchange coupling. In Fig. 1 are the spectra of Ti^{2+} doped into $MgCl_2$ and $MnCl_2$ [1]. In the former there is no exchange coupling while in the latter exchange interactions between Ti^{2+} and Mn^{2+} of the host lattice exist. The first two Ti^{2+} spin-allowed bands appear in both spectra at approximately the same energy with about the same intensity. (This and most of the other spectra referred to in this section will be discussed in more detail later.)

(2) Spin-forbidden d–d bands also appear at about the same energy in mononuclear and exchange-coupled systems. They show, however, notable changes in other details.

(a) The bands increase significantly in intensity in exchange-coupled systems. In Fig. 1 the $^3T_1 \rightarrow {}^1E$ transition of Ti^{2+} around 7700 cm^{-1} is seen

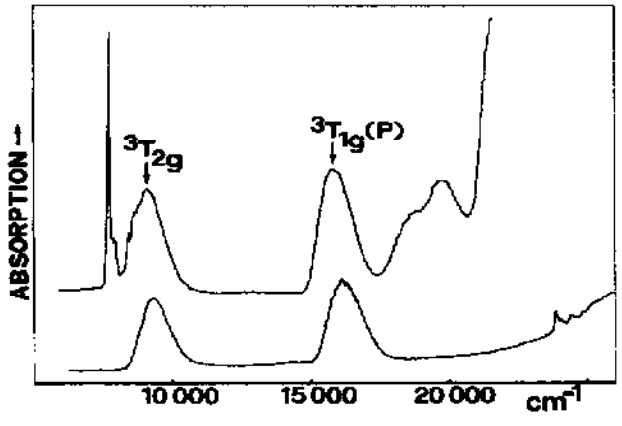

Fig. 1. Spectra at 10 K of Ti^{2+}-doped $MgCl_2$ (lower trace) and Ti^{2+}-doped $MnCl_2$ (upper trace). In the latter all bands below 17 500 cm^{-1} are due to Ti^{2+} [1]. (Reprinted with permission from Inorganic Chemistry. Copyright 1987 American Chemical Society.)

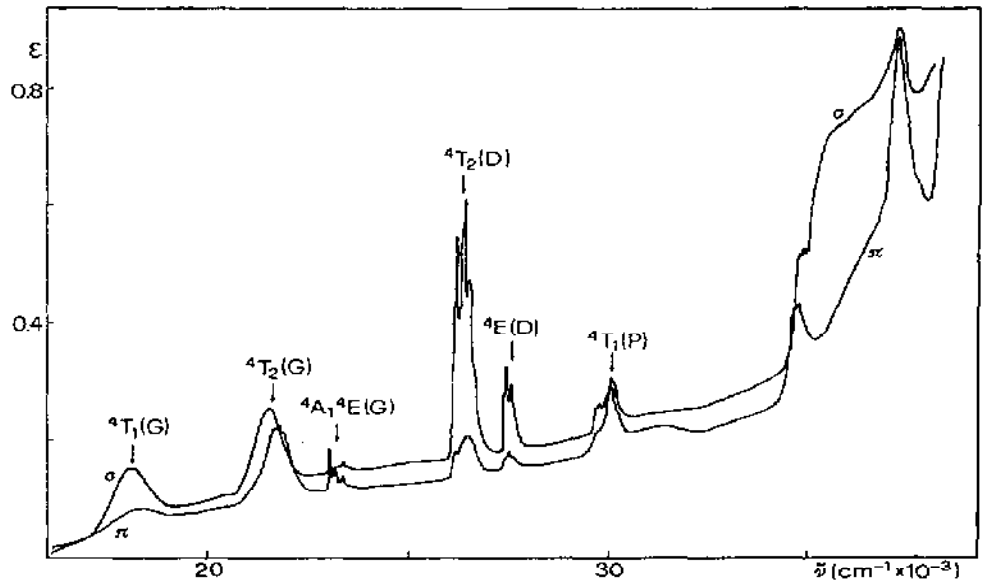

Fig. 2. Single-crystal absorption spectra of $CsMg_{0.80}Mn_{0.20}Br_3$ at 13 K. Octahedral labels are used although actual symmetry is trigonal [2]. (Reprinted with permission from Inorganic Chemistry. Copyright 1984 American Chemical Society.)

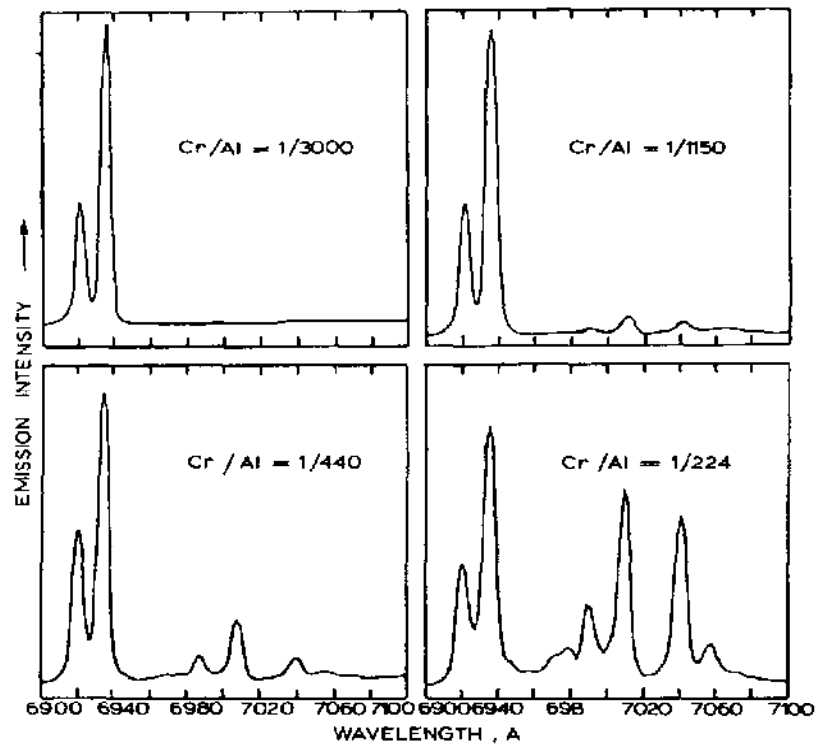

Fig. 3. Low resolution luminescence spectra of ruby (77 K) showing the appearance of pair lines with increasing Cr^{3+} concentration [3]. (Reprinted with permission from Physical Review Letters.)

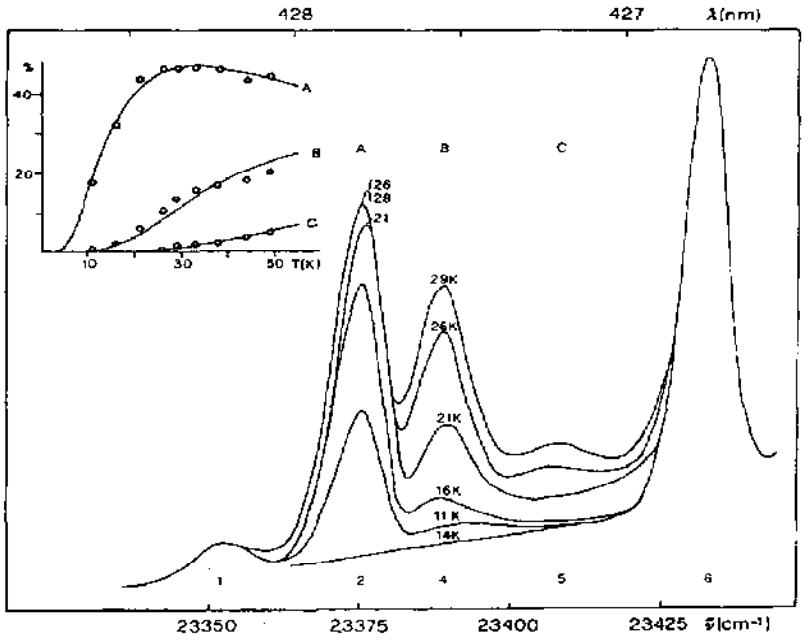

Fig. 4. Mn^{2+} pair and single-ion excitations (π) to $^4A_1(G)$ in $CsMg_{0.95}Mn_{0.05}Cl_3$. Inset: observed band areas and Boltzmann populations calculated with $2J = -19.6$ cm^{-1} [2]. (Reprinted with permission from Inorganic Chemistry, Copyright 1984 American Chemical Society.)

to be enormously enhanced in the $MnCl_2$ lattice. Likewise, the spectrum of exchange-coupled Mn^{2+} in $CsMg_{0.80}Mn_{0.20}Br_3$ (Fig. 2) [2], which consists entirely of spin-forbidden transitions, is between one and two orders of magnitude more intense than the spectrum of Mn^{2+} in aqueous solution. This is due to the presence of Mn^{2+} dimers, besides Mn^{2+} single ions, in this heavily doped mixed crystal.

(b) The bands often show additional fine structure. An example is the luminescence spectrum of ruby in the region of the $^4A_2 \leftrightarrow {}^2E$ excitations (Fig. 3) [3]. Besides the two dominant R lines of single Cr^{3+} centers there are a number of lines due to Cr^{3+} pairs, which increase in intensity as the Cr^{3+} concentration increases.

(c) Some spin-forbidden bands in exchange-coupled clusters show very noticeable temperature dependences. Figure 4 shows the π absorption spectrum of the $^6A_1 \rightarrow {}^4A_1$ region of $CsMg_{0.95}Mn_{0.05}Cl_3$ at various temperatures [2]. Several of the bands are seen to be hot bands, i.e. to vanish at very low temperatures. This indicates that the bands are due to Mn^{2+} pairs and that there is an electronic splitting of the ground state owing to exchange interactions.

(d) Often new absorptions appear at energies near the sum of the energies of two single excitations. An example of these double excitations can be seen

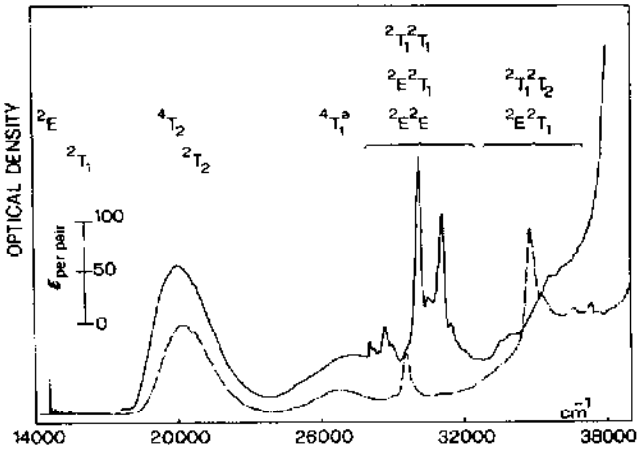

Fig. 5. Polarized absorption spectra at 15 K of {triol}$(ClO_4)_3$ in the region of $d-d$ transitions: solid trace (π); dotted trace (σ). Excitations designated in octahedral notation [4]. (Reprinted with permission from Molecular Physics.)

in Fig. 5 [4] for the complex $[LCr(OH)_3CrL](ClO_4)_3$ (L = 1,4,7-trimethyl-1,4,7-triazacyclononane) (abbreviated {triol}$(ClO_4)_3$). The sharp and prominent bands in the near UV are typical of exchange-coupled Cr^{3+} systems.

These then are the special spectroscopic features of exchange-coupled systems which need explanation and discussion.

(c) Theoretical models of exchange splittings

(1) Ground state. When dealing with orbitally non-degenerate, i.e. spin-only, ground state ions, the appropriate Hamiltonian is the well-known Heisenberg–Dirac–van Vleck operator:

$$\hat{H}_{gs} = -2J\left(\vec{S}_a \cdot \vec{S}_b\right) \tag{1}$$

The eigenvalues of eqn. (1) are easily obtained as

$$E(S) = -J\left[S(S+1) - S_a(S_a+1) - S_b(S_b+1)\right] \tag{2}$$

The energy splitting thus corresponds to a Landé pattern. A Hamiltonian of this type has been used since the 1930s by physicists to account for magnetic properties of solids. When the orbital moment is not completely quenched, eqn. (1) is no longer valid and more elaborate theoretical models containing more than one parameter are needed [5]. Very often eqn. (1) is used as a first approximation also in this situation, even though there is no theoretical justification for it.

Deviations from the simple Landé splitting pattern in eqn. (2) are sometimes observable when high resolution optical spectroscopy is used [6].

Empirically, a biquadratic term has been incorporated into eqn. (1) to account for such deviations:

$$\hat{H}_{gs} = -2J\left(\vec{S}_a \cdot \vec{S}_b\right) - j\left(\vec{S}_a \cdot \vec{S}_b\right)^2 \tag{3}$$

(It should be noted that in the literature various sign combinations are used in the two terms of this equation. Likewise, the coefficient 2 in the bilinear term is often omitted. In this review all data have been converted to conform to eqn. (3).) There are several physical effects which can lead to non-zero values of j. The most important are true biquadratic exchange and exchange striction. Both should lead to j values of the order of 1% of $|2J|$.

Mn^{2+} is a typical ion with a spin-only ground state ($^6A_1$), and we will here illustrate the effects with an Mn^{2+} pair. Mn^{2+} in its ground state has $S = 5/2$, and the coupled pair can thus have total spin $S = S_a + S_b$, $S_a + S_b - 1, \cdots, |S_a - S_b|$, i.e. $S = 5, 4, 3, 2, 1, 0$. The exchange interactions in the ground state are adequately described by eqn. (1), and eqn. (2) reduces to

$$E(S) = -J[S(S+1) - 35/2] \tag{4}$$

The corresponding splitting pattern for Mn^{2+} pairs in $CsMg_{0.95}Mn_{0.05}Cl_3$ is shown in Fig. 6 [2]. The symmetry labels are for the D_{3h} point group of the pair. The method for determining the labels is discussed by Day and Dubicki [7]. The population of the various ground state levels will be governed by a Boltzmann distribution. Accordingly, at very low temperature only the lowest level will be populated, while at higher temperatures the other levels can have a significant population. This, of course, depends on the value of J and the temperature.

(2) Excited states. When both ions of a pair are not in their ground state, the simple Hamiltonian (eqn. (1)) is in general no longer adequate. For an excited state derived from the same electron configuration as the ground state (spin-flip excitation) the following Hamiltonian, first proposed by Tanabe and coworkers [8–10], has proved to be adequate:

$$\hat{H}_{ex} = -2\sum_{ij} J_{ai\,bj}\left(\vec{s}_{ai} \cdot \vec{s}_{bj}\right) \tag{5}$$

where i, j number the singly occupied orbitals on the ions a and b respectively. $J_{ai\,bj}$ are orbital exchange parameters. They are related to J by

$$J = \frac{1}{4 \cdot S_a \cdot S_b} \sum_{ij} J_{ai\,bj} \tag{6}$$

In other words, J is simply the average of the orbital exchange parameters $J_{ai\,bj}$. (See Section B (iii) for further discussion of orbital exchange parameters.) Applied to the $^4A_1{}^6A_1$ excited state of our manganese pair, eqn. (5)

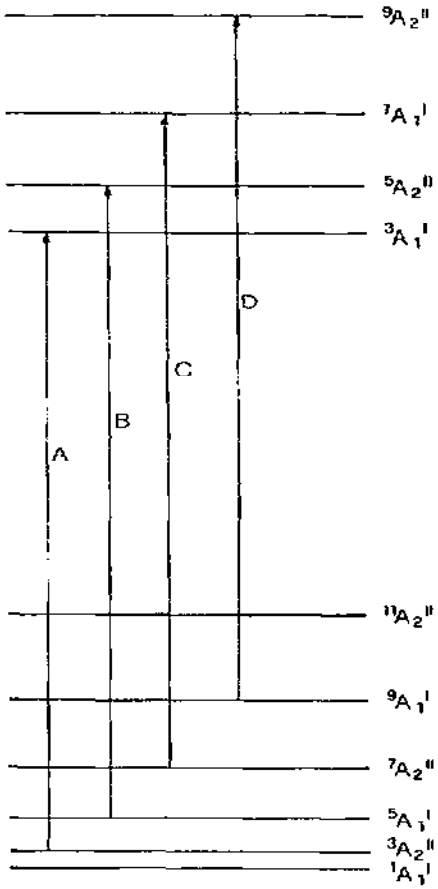

Fig. 6. Single excitations to $^4A_1{}^6A_1$ in $Mn_2Cl_9^{5-}$. The transitions are designated as in Fig. 4 [2]. (Reprinted with permission from Inorganic Chemistry. Copyright 1984 American Chemical Society.)

leads to the energy splitting pattern shown in Fig. 6. As a result of the orbital non-degeneracy of $^4A_1$, we obtain a Landé splitting pattern as in the ground state. This is a very special situation which, of course, is described by a simple Hamiltonian such as eqn. (1). If, however, we take the $^4E^6A_1$ excited states of an Mn^{2+} pair or the $^2E^4A_2$ excited states of Cr^{3+} dimers, which will be discussed in detail below, the situation can only be described by eqn. (5).

As will be discussed in the following section, exchange-induced electronic excitations follow the spin selection rule, $\Delta S = 0$. In an Mn^{2+} pair we might expect to see one to four hot absorption bands corresponding to $\Delta S = 0$. The intensities of the bands will depend on the transition moments and on the temperature-dependent population of the ground state levels. As the temperature is lowered, the ground state population shifts largely to the $S = 0$ level. Since there is no $S^* = 0$ excited state, all the bands will decrease

in size and eventually vanish if the temperature is lowered sufficiently. This is seen in Fig. 4. The bands A, B, C correspond to the transitions marked in Fig. 6. The $S = 4 \rightarrow S^* = 4$ pair absorption probably lies under the single-ion band at 23433 cm^{-1}. The Boltzmann populations can be calculated for various values of J and then compared with the band areas at various temperatures. The best fit in this case is with $2J = -19.6$ cm^{-1}, as is seen in the inset in Fig. 4.

The structure of $CsMgCl_3$ consists of infinite chains of face-sharing octahedra, each of which contains an Mg^{2+} surrounded by six Cl^- [11]. The $Mn_2Cl_9^{5-}$ pairs which exist in the mixed crystal will have D_{3h} symmetry, and spectra can be recorded with $\vec{E} \perp c(\sigma)$ or $\vec{E} \| c(\pi)$, where c is the threefold axis. From the symmetry of the various ground and excited pair states, it is readily shown that the pair transitions discussed here should be π polarized, and indeed are found to be almost completely so.

If the splittings for the excited state were the same as for the ground state, all the absorption curves A, B and C in Fig. 4 would coincide. Since the curves are not superimposed, their spacings can be used to estimate how much greater or smaller the excited-state separations are than those in the ground state. From this, a value can be assigned to an effective coupling constant J_{ex} for the particular excited state being studied. In the present case the line spacings indicate that $2J_{ex}$ is -26.8 cm^{-1}, as compared with $2J = -19.6$ cm^{-1} in the ground state.

J_{ex} is often found to be 20%–50% higher than J for the ground state, as is the case here. A possible reason is the following. According to quantum mechanics, antiferromagnetic exchange interactions have their origin in metal-to-metal or ligand-to-metal electron-transfer processes [9]. The energies of the relevant electron-transfer states are usually not known, but are assumed to be between 50000 and 100000 cm^{-1}. In terms of simple perturbation theory it is thus plausible that singly or doubly d–d excited pair states can acquire more electron-transfer character than the pair ground state. As a consequence, the corresponding J values are higher.

(ii) Intensity mechanisms and selection rules

(a) Example

One of the most striking features of the spectra of exchange-coupled systems is the great enhancement, often by more than two orders of magnitude, of the intensity of spin-forbidden bands. As an example, we refer again to Fig. 1 which shows the spectrum of Ti^{2+} in $MgCl_2$ and $MnCl_2$. The titanium spin-forbidden transition to the lowest excited singlet state, $^3T_1 \rightarrow {}^1E$ (octahedral notation), is at least two orders of magnitude more intense in the latter matrix than in the former, where it is too weak to

be measured. In $MnCl_2$ there is exchange coupling between Ti^{2+} and its six nearest Mn^{2+} neighbors. We will treat this spectrum more in detail in Section B (v). For the present we will discuss only the reasons why exchange coupling brings about this intensity enhancement. Two principal mechanisms for the intensity of spin-forbidden transitions need to be considered, the single-ion mechanism and the exchange mechanism.

(b) Mechanisms

In general, d–d transitions need some odd-parity field to make them electric-dipole allowed. This can be provided either by a static ungerade ligand-field potential or by vibronic coupling involving an ungerade vibration. In addition, for the spin-forbidden bands, the $\Delta S = 0$ restriction can be overcome by spin–orbit coupling. While an individual ion may lie on a center of symmetry, the constituent ions of a dimer cannot be so situated, and thus will necessarily be in an odd-parity ligand field. In an extended magnetic system, however, a metal ion may well lie on a center of inversion, as is the case for Mn^{2+} in $CsMnBr_3$ (symmetry D_{3d}). The single-ion mechanism can provide intensity to a transition also in an exchange-coupled pair. This mechanism does not, however, provide an intensity enhancement compared with uncoupled single ions of comparable ligand-field potential. For the single-ion mechanism, in addition to the selection rules determined from orbital symmetry, the spin selection rules for the pair are $\Delta S = 0, \pm 1$ and $\Delta M_S = 0, \pm 1$ [9].

The exchange mechanism has been elaborated by Tanabe and coworkers [8–10]. A pair of ions can couple through the interaction of the electric vector ($\vec{E}$) of the incident light. For a pair whose electrons are in the singly occupied orbitals a_i and b_j the interaction is expressed as [12]

$$\hat{H} = \sum_{ij} \left(\vec{\Pi}_{a_i b_j} \cdot \vec{E}\right)\left(\vec{s}_{a_i} \cdot \vec{s}_{b_j}\right) \tag{7}$$

The vector components of the coefficients in the summation are

$$\Pi^{\alpha}_{a_i b_j} = 2\left\{\left(\partial J_{a_i b_j}\right)/\partial E^{\alpha}\right\}_{E^{\alpha}\to 0} (\alpha = x,\ y,\ z) \tag{8}$$

where $J_{a_i b_j}$ are the off-diagonal elements in the exchange-interaction matrix between the ground and the excited pair state. For this mechanism the spin selection rules for the pair are $\Delta S = 0$ and $\Delta M_S = 0$. There are, in addition, selection rules given by the orbital parts of the pair wavefunctions. This second mechanism turns out to be most effective for pure spin-flip transitions such as the ${}^4A_2 \to {}^2E$ transition of Cr^{3+}, or the ${}^6A_1 \to {}^4A_1, {}^4E$ transitions of Mn^{2+}, our example in the previous section.

It is important to note that the same mechanisms are involved in exchange-coupled clusters as in magnetically ordered insulating materials. In the latter, phenomena such as magnon sidebands, which correspond to the

simultaneous excitation of an exciton and a magnon, require concepts from solid state physics for their elucidation. The relevant interactions are, however, essentially those between nearest neighbors, i.e. pairwise interactions. Therefore, a theory for a pair is relevant also for the systems with extended interactions. This is also one of the main reasons that dimers and small clusters are useful molecular models for the more complicated magnetic materials with extended exchange interactions in one, two or three dimensions.

In actual spectra, contributions are usually found from both intensity mechanisms. For example, the emission spectrum of $[(NH_3)_5CrOHCr(NH_3)_5]Cl_5 \cdot H_2O$ (abbreviated $\{rhodo\}Cl_5 \cdot H_2O$) is shown in Fig. 7(a) [6]. The nature of the three spectra in this figure will be discussed in Section C (iii). At present, it is sufficient to note that all the bands originate in the $^5B_1$ level (C_{2v} notation) of the $^2E^4A_2$ excited state of the exchange-coupled pair, and that the strongest emission line is to the $^5A_1$ ground state level. For this transition $\Delta S = 0$ and the intensity is largely exchange induced. The weaker bands on either side are $^5B_1 \rightarrow {}^7B_2$ and $^5B_1 \rightarrow {}^3B_2$; both have $\Delta S = |1|$ and their intensity is due to a single-ion mechanism. The very weak doubly spin-forbidden transition $^5B_1 \rightarrow {}^1A_1$ is about three orders of magnitude weaker. Its appearance cannot be accounted for by the above-mentioned mechanisms. It is most likely due to anisotropy effects, which have been completely neglected in our discussion so far.

An illustrative way to distinguish between a single-ion mechanism and an exchange mechanism is by magnetic circular dichroism (MCD) or the analogous magnetic circularly polarized luminescence (MCPL). Both these phenomena require transitions for which $\Delta M_S = \pm 1$. Such transitions cannot occur by an exchange intensity mechanism ($\Delta S = 0$, $\Delta M_S = 0$). Exchange-induced absorption or emission bands should therefore exhibit no MCD or MCPL signals. In contrast, pair transitions arising from a single-ion mechanism can have $\Delta M_S = \pm 1$ and thus be MCD and MCPL active. This is illustrated in Fig. 7(b) [6]. The $\Delta S = 0$ pair bands, which are dominant in intensity, have no MCPL, whereas the two $\Delta S = \pm 1$ transitions do have it. The situation is more complicated when a pair transition has both single-ion and exchange-induced intensity. The two transition dipoles can interfere and as a result $\Delta S = 0$ and $\Delta M_S = 0$ transitions may be MCD active. An example is given by the ^4E, $^4A_1$ excitations of Mn–Ni pairs in $KZnF_3$ [13].

(iii) Orbital exchange parameters and exchange pathways

The well-known Kanamori–Goodenough rules [14,15] have been very successful in correlating in a qualitative way the magnetic properties with the structural properties of a large number of transition metal compounds.

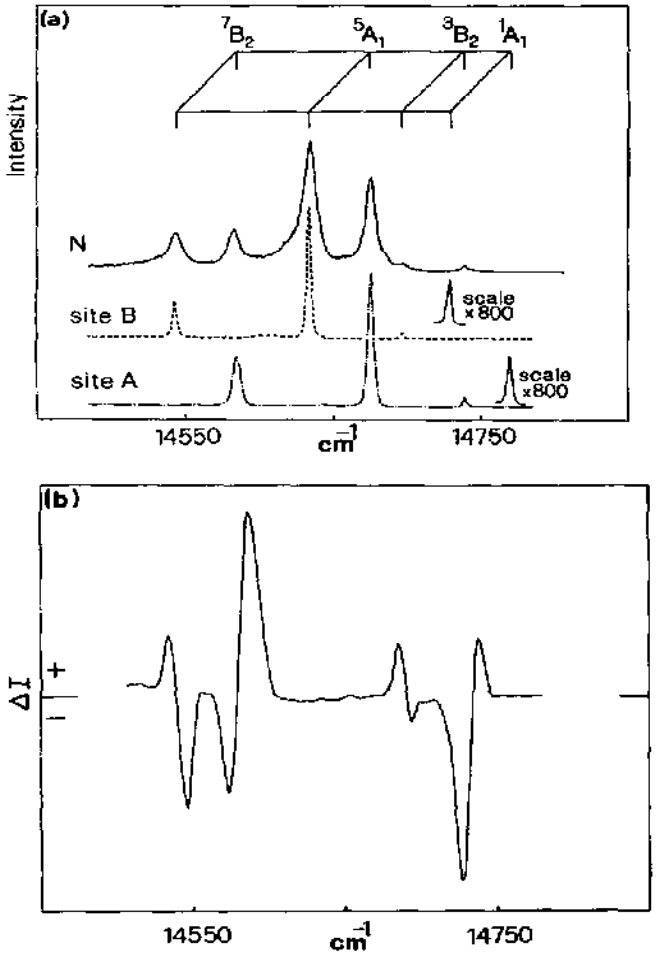

Fig. 7. (a) Site-selective luminescence spectra of {rhodo}$Cl_5 \cdot H_2O$ at 1.5 K. Sites A and B were excited at 14862 and 14821 cm^{-1} respectively. Spectrum N was obtained by non-selective excitation with the 514.5 nm Ar^+ laser line. Assignments to the exchange-split ground levels are included. (b) Non-selectively excited MCPL spectrum of the same compound in the same range at 4.2 K [6]. (Reprinted with permission from Molecular Physics.)

They are based on the concept of orbital exchange parameters. The total or overall exchange parameter J is composed of orbital contributions, some of which may be dominant, depending on the electron configuration and the bridging geometry of the dimer.

In a study of ground state properties, only the overall exchange parameter can be determined. Information about orbital contributions to J can only be obtained from a comparison of compounds with related structures and different electron configurations, or with the same electron configuration and different structures.

For a description of exchange interactions in an excited state such as $^2E^4A_2$ (single excitation) or $^2E^2E$ (double excitation) in Cr^{3+} dimers, or $^4E^6A_1$ of an Mn^{2+} dimer, a Heisenberg Hamiltonian is not appropriate. As shown in Section B (i), the relevant Hamiltonian (eqn. (5)) contains the orbital exchange parameters, $J_{ai\,bj}$, which average to J, the overall exchange parameter (eqn. (6)). The exchange splitting pattern in these excited states is therefore not a simple Landé pattern, and it has accordingly a higher information content than the ground state pattern, which can be described by the single parameter J. Individual $J_{ai\,bj}$ parameters, and thus the orbital pathways of the exchange, can be determined by analyzing the exchange splittings in the excited states. In principle, therefore, optical spectroscopy can yield information about the mechanisms of exchange which are not obtainable from a study of the ground state properties only.

Several studies of Cr^{3+}-doped oxide lattices (see also Section D (i)) contain values for the various orbital exchange parameters. Among these are the reports on Cr^{3+} in $GdAlO_3$ [16], $LiGa_5O_8$ [17], $ZnGa_2O_4$ [18] and ruby [12]. Orbital exchange parameters have also been reported for molecular Cr^{3+} complexes, such as the singly bridged $\{rhodo\}Cl_5 \cdot H_2O$ [6] and $[(NH_3)_5CrOHCr(H_2O)(NH_3)_4]Cl_5 \cdot H_2O$ (acid erythro chloride) [19], the doubly bridged $[(NH_3)_4Cr(OH)_2Cr(NH_3)_4]Br_4 \cdot 4H_2O$ and related compounds [20–22], and the triply bridged $\{triol\}(ClO_4)_3$ [4]. Data for $Cr_2Cl_9^{3-}$ [23], $Cr_2Br_9^{3-}$ [24,25] and $Mo_2Cl_9^{3-}$ [26] have also appeared. (See ref. 22 for a discussion of the trends in the parameters in various $M_2X_9^{3-}$ dimers.) Orbital exchange parameters for Mn^{2+} pairs in $KMgF_3$ and $KZnF_3$ were discussed in the early pioneering work of Ferguson, Tanabe and coworkers (for example, see refs. 8 and 27), and are also treated for Mn^{2+} pairs in $CsMgX_3$ (X = Cl, Br) [2] and CdX_2 (X = Cl, Br) [28]. V^{2+} pairs in $CsMgCl_3$ have also been discussed in this regard [29].

An example can be taken from the spectra of di-μ-hydroxo-bridged Cr^{3+} complexes. A large number of complexes having two OH or two OR bridges have been magnetically characterized [30]. The values of $2J$ span a range from $+2$ to -43 cm^{-1}. J was found to vary significantly for the same complex in different salts, i.e. in different crystal environments. The tilt angle of the OH or OR bond out of the CrO_2Cr plane was found to be an important parameter. A very detailed study of $[(en)_2Cr(OH)_2Cr(en)_2]Br_4 \cdot 2H_2O$, $[(NH_3)_4Cr(OH)_2Cr(NH_3)_4]Br_4 \cdot 4H_2O$ and their chloro analogs has been reported [20,21]. Of the two possible orbital exchange pathways, in-plane and out-of-plane, the latter was found to provide the dominant antiferromagnetic contribution (see Fig. 8) [31]. Out-of-plane interaction involves d_{xz} and d_{yz} orbitals on the magnetic ions and p_z orbitals on the bridging oxygen atoms (z axis perpendicular to the molecular plane) in a superexchange pathway. This orbital parameter, $J_{xz\,yz}$, was drastically re-

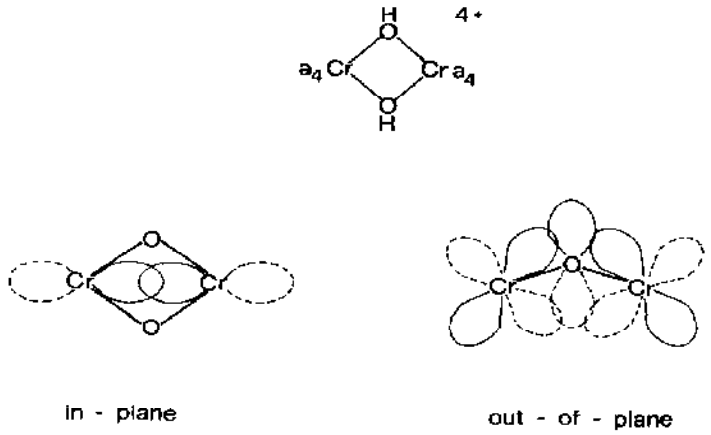

Fig. 8. Exchange interaction pathways in $[a_4Cr(OH)_2Cra_4]^{4+}$ complexes [31]. (Reprinted with permission from ACS Symposium Series. Copyright 1986 American Chemical Society.)

duced from -145 to -55 cm^{-1} on going from the en–Br to the NH_3–Br compound. There is good correlation with the crystal structure, since the OH tilt angle is 6° in the former and 55° in the latter. In the former the p_z oxygen orbital is almost fully available for electron transfer and kinetic exchange. In the latter, however, the bonding situation at the oxygen is more sp^3-like, and the p_z orbital is thus no longer fully available for exchange. This is in good agreement with the conclusions reached by Glerup et al. [30] on the basis of the magneto-structural correlations in the whole diol series.

The antiferromagnetic part of the parameter $J_{a_i\,b_j}$ can be related to the one-electron transfer integral from orbital ai to orbital bj, which is proportional to the energy difference between the dimer orbitals obtained from the plus and minus combinations of the i and j magnetic atomic orbitals. Extended Hückel MO calculations can be used to estimate these energy differences [32]. The result of such a calculation on $[(en)_2Cr(OH)_2Cr(en)_2]^{4+}$ is in reasonable quantitative agreement with the experimentally determined orbital parameters [22]. The dominance of the out-of-plane exchange pathway via oxygen clearly comes out of the calculation.

(iv) Double excitations

The spectra of exchange-coupled systems often show sharp intense bands at high energy, which in many cases can be assigned to double excitations. In these processes a single photon simultaneously excites both metal ions in the coupled dimer. As an example we refer again to Fig. 5, which shows the absorption spectrum of $\{triol\}(ClO_4)_3$. The bands appear at an energy approximately equal to the sum of the energies of the spin-forbidden single excitations in the near IR, and they are considerably more intense than the

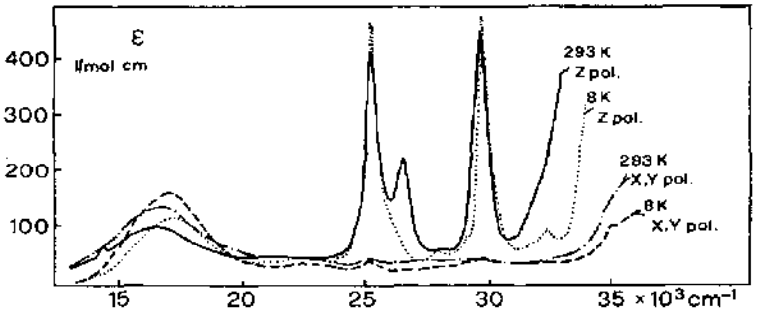

Fig. 9. Polarized crystal absorption spectra of basic rhodo perchlorate at 8 and 293 K [33]. (Reprinted with permission from Chemical Physics.)

single excitations. The exchange-coupling formalism suggested by Tanabe and coworkers [8–10] can also be employed here. In the case of a Cr^{3+} dimer such as we have here, the ground state ($^4A_2{}^4A_2$) will have levels with total spin $S = 0, 1, 2, 3$. The singly excited dimer states (e.g. $^2E{}^4A_2$) will have $S^* = 1, 2$. The doubly excited dimer states (e.g. $^2E{}^2E$) will have $S^* = 0, 1$. Thus there will be formally allowed double excitation bands with $\Delta S = 0$. Even at very low temperatures when only the $S = 0$ ground level is occupied these bands will be seen in the spectra. This contrasts with the single excitations, where only hot bands can have $\Delta S = 0$.

The intensity enhancement of the double excitations compared with the single excitations is very conspicuous, being one to two orders of magnitude. This can be partly, but only partly, explained by the proximity of the intensity-donating charge-transfer transitions using the ideas of perturbation theory. Exchange interactions and exchange-induced intensity have their roots in, and are related to, electron-transfer processes. Of these, one-electron ligand-to-metal and metal-to-metal transfers are the most important [8,9]. The excited pair states can acquire some character of these electron-transfer states. Since the doubly excited states lie closer to these, the mixing will be stronger and thus the intensity enhancement greater.

Another example of double excitation is shown in Fig. 9 [33]. The compound $[(NH_3)_5CrOCr(NH_3)_5](ClO_4)_4$, basic rhodo perchlorate, contains a relatively strongly coupled dimer with $2J = -450$ cm^{-1}. The visible/near-UV spectrum is dominated by the prominent and relatively sharp double excitations. They have ϵ values up to 400, thus exceeding those of the spin-allowed $^4A_2 \rightarrow {}^4T_2$, $^4T_1$ Cr^{3+} excitations. These bands had been detected early on in the solution spectrum of basic rhodo. They give the solution an intense blue color, atypical of "normal" Cr^{3+} complexes, and there was considerable speculation as to their nature. Numerous theoretical models for the supposedly "strong" coupling in this dimer were advanced (see references in ref. 33). It is clear, however, that with $2J = -450$ cm^{-1}

the coupling is weak compared with all the relevant single-ion interactions. This is also evident from the absorption spectrum, which shows the typical features of a Cr^{3+} complex but with the very intense double excitations added to it. A single-crystal absorption spectrum furnished the clue to understanding these strange bands. They were found to be completely polarized along the Cr–Cr axis, and a vibronically induced Tanabe mechanism was suggested for their interpretation [33]. The same mechanism was later invoked to explain the symmetrical $^6A_1{}^6A_1 \rightarrow {}^4E{}^4E$ and $^4A_1{}^4A_1$ double excitations of Mn^{2+} pairs in $KMgF_3$ [34].

Tsuboi and Kleeman [35] noted three bands between 225 and 260 nm in the 4.5 K spectrum of $BaMnF_4$ which they assign to double excitations. For example, the $^4T_1$ state lies at ~ 530 nm, and the band at ~ 260 nm is assigned to the double excitation to this state. Several examples of ^2E and $^2T_1$ double excitations in the spectra of ruby [36], and of Cr^{3+} doped into $LaAlO_3$ [16] and $YAlO_3$ [37] have been reported by van der Ziel. Double excitations have also been observed in the spectra of magnetically coupled lanthanide compounds (see Section D (viii)).

The above discussion has been limited to double excitations which involve transitions which are spin forbidden in the single ion. Considerably less is understood about those which involve transitions which are spin allowed in the single ion. In a number of spectra of exchange-coupled $3d$ transition metal systems, however, broad bands have been observed which have no counterpart in the single-ion spectrum, and which therefore have to be attributed to interactions between the magnetic ions. A common feature of all of these is that they occur at energies which are approximately the sum of two spin-allowed excitations. Therefore an obvious, and in some cases the only reasonable, assignment is that of double excitations. However, it must be noted that the mechanism by which they acquire intensity is by no means clear. It is not by a normal Tanabe mechanism, which applies to spin-forbidden bands. The most notable examples are the typical "dimer bands" in Cu^{2+} dimers, discussed in Section D (iv) of this review. As noted there, however, the assignment as double excitations appears to be less favored than a ligand-to-metal charge-transfer assignment.

In VCl_2 and $KVCl_3$ unusually intense bands are found at higher energies [38,39]. Specifically, we can see in the reported spectra that the three bands assigned to the usual ligand-field spin-allowed transitions decrease in size on cooling from room temperature to 77 or 4.2 K. Three other bands with intensities like those of the ligand-field bands lie at higher energies. In VCl_2 at least two ($\sim 25\,500$ and $\sim 28\,000$ cm^{-1}) increase in size on cooling to 4.2 K. One of these latter may therefore be a double excitation, since the $^4T_1(F)$ lies at 14 000 cm^{-1}. In the spectra of $CsVX_3$ (X = Cl, Br, I) [40], in addition to the usual ligand-field bands, there are strong double excitations of

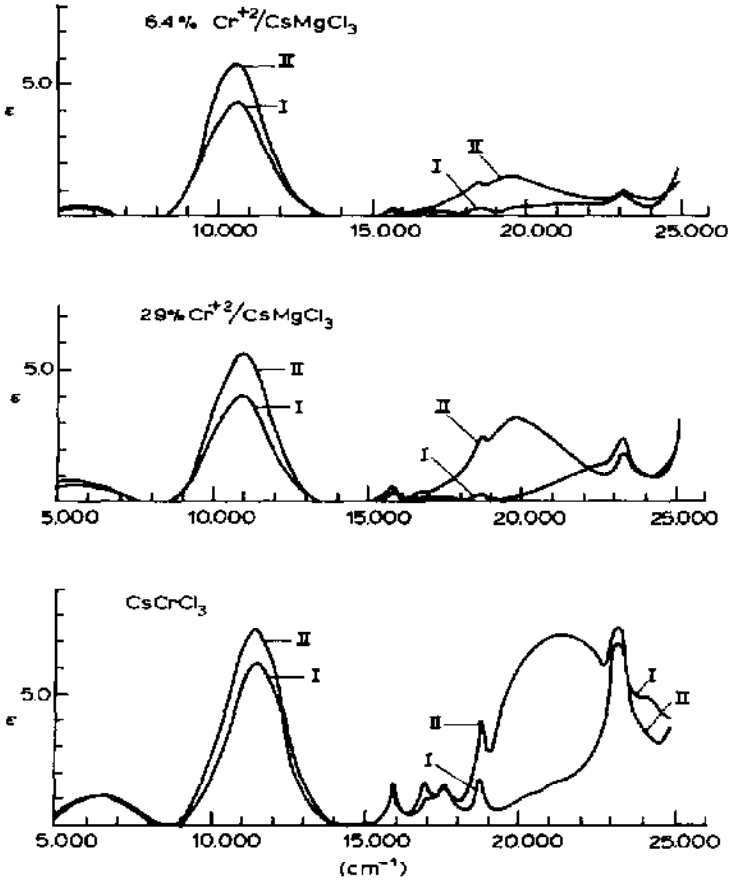

Fig. 10. Polarized crystal absorption spectra of $CsCrCl_3$ and $CsMgCl_3$ doped with Cr^{2+} at 77 K [41]. (Reprinted with permission from Journal of Chemical Physics.)

spin-forbidden transitions as well as a weak broad band at 19780 (Cl), 17570 (Br) and 15450 cm^{-1} (I), which increases in intensity on cooling. The band is completely π polarized (along the V–V axis), and lies at approximately twice the energy of the lowest spin-allowed band ($^4T_2$). These facts suggest that it is a double exciton involving $^4T_2$. It is not clear, however, by which mechanism it acquires its almost pure π intensity.

A very clear example of double excitation involving spin-allowed transitions is seen in Fig. 10 [41], in which the spectra of $CsCrCl_3$ and $CsMgCl_3$ doped with Cr^{2+} are shown. The spectrum of Cr^{2+} shows one spin-allowed band, $^5E \rightarrow {}^5T_2$ (octahedral notation), around 11000 cm^{-1}. At approximately twice this energy is a band whose intensity increases with Cr^{2+} ion concentration and which is completely π polarized, i.e. along the Cr–Cr axis. Both bands shift to higher energy as the Cr^{2+} concentration increases. This appears to be due to different ligand-field strengths in the different

lattices. These observations led the researchers to assign the higher energy band to a simultaneous excitation of two Cr^{2+} ions to the $^5T_2$ state.

Several reports note anomalously intense high energy bands in various spectra. Often the bands lie in the same range calculated for spin-forbidden bands, and therefore have most often been so assigned. For example, the spectra of K_2CoF_4 and Rb_2CoF_4 show a broad band of moderate intensity, stronger in σ than in π, around 40 000 cm^{-1} [42]. This is about twice the energy of the $^4T_1(P)$ transition. It was not assigned by the researchers as a double excitation, but may well be one. Similar effects were also found in the spectra of $KCoF_3$ [43] and $KNiF_3$ [44]. In the latter case successive substitution of Mg^{2+} for Ni^{2+} caused the anomalous intensity to disappear. The spectrum of $KNiF_3$ [45] shows the $^3T_1$ band at 24 300 cm^{-1} and the moderately intense UV band at 48 500 cm^{-1}.

(v) "Spin clusters"

In addition to the substitution of paramagnetic ions into diamagnetic lattices, these ions can be substituted as impurities in lattices which are themselves magnetic. The impurity ion can form a "spin cluster" with its nearest-neighbor magnetic ions, and the spectra of the impurity ion may then reflect its interactions with the lattice spins. We will outline an example [1] which illustrates the unusual spectroscopic effects and interprets them using a simple theoretical cluster model.

Ti^{2+}, a d^2 ion, is doped into $MnCl_2$, which is a layer lattice with the $CdCl_2$ structure, and which orders antiferromagnetically to complex three-dimensional magnetic phases at 1.96 and 1.81 K [46]. Each Ti^{2+} has six nearest-neighbor Mn^{2+} ions within the magnetic layer. The axial absorption spectrum of crystalline $Mn_{0.99}Ti_{0.01}Cl_2$ (Fig. 1) shows absorptions due to Ti^{2+} between 7500 and 17 500 cm^{-1} and those due to Mn^{2+} above 17 500 cm^{-1} [1]. The titanium spectrum shows the two lowest spin-allowed d–d bands at 9090 and 15 820 cm^{-1} (10 K), as well as the $^3T_1 \rightarrow {}^1E$ transition with the strongest peak at 7773 cm^{-1} (1.5 K). The analogous spectrum at 10 K of $Mg_{0.99}Ti_{0.01}Cl_2$ (Fig. 1) shows only the two broad spin-allowed bands at 9440 and 16 390 cm^{-1} with no evidence of the triplet–singlet absorption [47]. The $^3T_1 \rightarrow {}^1E$ excitation in the $MnCl_2$ lattice is enhanced by a factor of approximately 400 as estimated from the $^1E \rightarrow {}^3T_1$ radiative emission lifetimes [48]: τ for Ti^{2+} in $MgCl_2$ at 13 K is 125 ms, and τ for Ti^{2+} in $MnCl_2$ at 15 K is 327 μs.

Figure 11 [1] shows in greater detail the region of the sharp absorption band and the corresponding emission. It also contains some results of the spin-cluster model calculation which will now be briefly outlined. Each Ti^{2+} ($S = 1$) can magnetically couple with six nearest-neighbor Mn^{2+} (each with

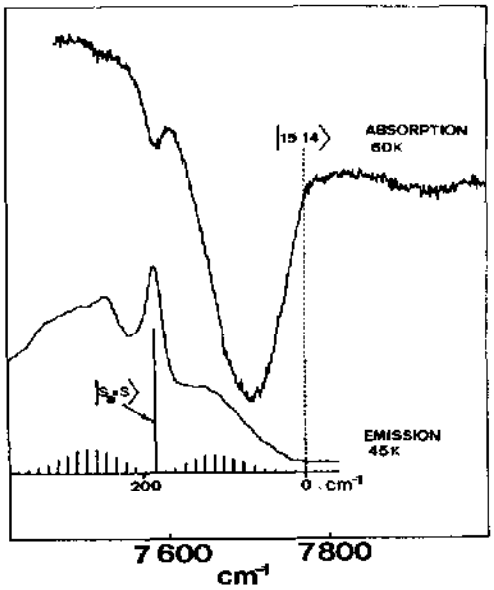

Fig. 11. Emission spectrum (45 K) and inverted absorption spectrum (60 K) of $MnCl_2$ doped with Ti^{2+} in the region of ${}^3A_2 \leftrightarrow {}^1E$ transitions. Broken vertical line marks the lowest energy ground state level. The inset at bottom shows the ground state exchange splitting pattern of the $Ti(Mn)_6$ cluster including degeneracies [1]. (Reprinted with permission from Inorganic Chemistry. Copyright 1987 American Chemical Society.)

$S = 5/2$). The Mn^{2+}–Mn^{2+} interaction is known to be of the order of 1 cm^{-1} [28], while that of the Ti^{2+}–Mn^{2+} is expected to be larger. An important assumption in the spin-cluster model is that the latter exchange dominates the former. The ground state of the Ti^{2+} ion in this crystal is ${}^3A_2$ (D_3 notation); the trigonal ${}^3E$ component lies several hundred wavenumbers higher in energy [49]. This means that the ground state is an orbital singlet. Since Mn^{2+} also has an orbitally non-degenerate ground state (${}^6A_1$ in D_3), the simple Heisenberg operator will apply. If we neglect the Mn^{2+}–Mn^{2+} coupling, the interaction can be simply expressed as

$$\hat{H}_{\text{cluster}} = -2J\left(\vec{S}_0 \cdot \vec{S}_a\right) \tag{9}$$

where $\vec{S}_0$ is the spin of Ti^{2+} and $\vec{S}_a$ is the total spin of the six nearest-neighbor Mn^{2+} ions. S_a ranges from 0 to 15 and $S_0 = 1$. The eigenfunctions of this operator can be designated $|S_a\ S>$, where S is the total cluster spin, with the following energies:

$$E(S_a,\ S) = -J\left[S(S+1) - S_a(S_a+1) - S_0(S_0+1)\right] \tag{10}$$

There will then be 32 equally spaced cluster levels with an energy interval of $2J$ and with various high degeneracies. The energy splitting pattern and the "density of states", i.e. the degeneracies, are shown in Fig. 11. The level with

the singularly high degeneracy of 46 656 corresponds to $S = S_a$, and the higher and lower energy wings to the $S = S_a - 1$ and $S = S_a + 1$ levels respectively.

The lowest excited state of Ti^{2+} is ^1E (D_3 notation). This singlet state has zero spin so that $S = S_a$. Therefore, if Mn^{2+}–Mn^{2+} exchange is neglected, in this excited state the cluster has a single highly degenerate energy level. The transitions to this single level from the various cluster levels of the ground state are those that are seen in the absorption spectrum. The intensities of the components, corrected for Boltzmann factors, are expected to be proportional to the degeneracies of the ground levels. It is seen in Fig. 11 that this is approximately correct. The sharp hot peak (7586 cm^{-1}) originates in the highly degenerate ground level ($S = S_a$).

The value of J_{Ti-Mn} can be estimated from the position of the sharp cold band observed at 7773 cm^{-1} in the 1.5 K absorption spectrum, and the sharp hot band at 7586 cm^{-1}. Since these transitions correspond to the $|15\ 14>$ and $|S_a = S>$ ground state levels respectively, their difference can be equated to $30J$, leading to $2J = -12.4$ cm^{-1}.

The 45 K luminescence spectrum nicely conforms to this spin-cluster picture, as shown in Fig. 11. It should be noted, however, that at very low temperature the luminescence spectrum is quite complex, developing a large number of sharp bands and bearing no resemblance to the corresponding absorption spectrum. This most unusual behavior is one of the most interesting aspects of this system. A quantitative analysis is not yet available, but the explanation seems to lie in the following direction. In the excited ^1E state the Ti^{2+} has no magnetic moment. At low temperature as the two-dimensional antiferromagnetic ordering of $MnCl_2$ is approached, the Mn^{2+} spins will order as a result of Mn^{2+}–Mn^{2+} exchange. The Ti^{2+} magnetic moment is created in the emission process. This process is too fast for the neighboring Mn^{2+} spins to follow. Thus the new Ti^{2+} spin finds itself in a surrounding determined by the Mn^{2+} magnetic order. This is not the cluster ground state. Therefore there is no correlation between absorption and emission below 4 K, where the two-dimensional magnetic order of $MnCl_2$ sets in. Non-radiative relaxation into the cluster ground state takes place afterwards.

A system which has been studied in detail is Cr^{3+} doped into the antiferromagnet, $GdAlO_3$ [50–53], for which $T_N = 3.9$ K [52]. In this nearly perfect perovskite, Al^{3+} (and Cr^{3+} which may replace it) is surrounded by eight Gd^{3+}. The interaction of Cr^{3+} ($S = 3/2$) with the eight Gd^{3+} (each with $S = 7/2$) causes the spectra, especially of the $^4A_2 \rightarrow {}^2E$ transition, to differ noticeably from the spectra of Cr^{3+} in the diamagnetic perovskite host, $LaAlO_3$. Stronger deviations are seen in luminescence than in absorption. The theoretical interpretation of these results is rather involved. Ab-

sorption and emission measurements of the $^4A_2 \rightarrow {}^2E$ transitions at 4.2 K in magnetic fields up to 6 T have been reported for this system. The Cr^{3+}–Gd^{3+} exchange-coupling constant varies from -2.1 cm^{-1} (zero field) to -1.46 cm^{-1} (high field) [54] (see this reference for earlier work on this system).

Van der Ziel and van Uitert have studied the emission and absorption spectra of Cr^{3+}-doped $EuAlO_3$ [55,56]. Owing to the exchange coupling between the two ions, bands were seen which correspond to collective excitation of the Cr^{3+} ($^4A_2 \rightarrow {}^2E$) and of the Eu^{3+} ($^7F_0 \rightarrow {}^7F_1$), as well as difference bands due to cross-relaxation, i.e. the simultaneous excitation of Cr^{3+} and de-excitation of Eu^{3+}. The latter bands are weak, since they depend on the thermal population of $^7F_1$. Analogous effects were also found in the luminescence spectra.

Aoyagi et al. [57] have studied Cr^{3+} in $Dy_3Al_5O_{12}$ (dysprosium aluminum garnet). They found they could account for the fine structure associated with the R lines by taking into account the exchange interaction between the Cr^{3+} and the surrounding Dy^{3+} spins. They also give references to the spectra of Cr^{3+} in the analogous yttrium aluminum garnet. The absorption and luminescence of antiferromagnetic garnets with Cr^{3+} in octahedral sites have also been reported [58].

Ferre and Regis [59] have studied the spectrum of $K_2Cu_{1-x}Mn_xF_4$ where $x < 100$ ppm. From the structure and temperature dependence of the sharp ^4E and $^4A_1$ Mn^{2+} excitations they derived, using a spin-cluster model, a value of $2J = -52 \pm 2$ cm^{-1} for the Mn^{2+}–Cu^{2+} interaction.

Another system that has been studied in absorption is Ni^{2+} substituted in MnI_2 [60]. The spectra of Rb_2CrCl_4 containing 1.8% and 3.8% Mn^{2+} have also been reported [61], as well as the spectra of the mixed system, $KMn_xNi_{1-x}F_3$ [62].

C. SPECTROSCOPIC TECHNIQUES

(i) Single-crystal polarized absorption spectroscopy

Absorption spectroscopy is the most fundamental of the techniques that are used in this field. To obtain the most information from it, however, we must know the orientation within the crystal of the chromophore, which in our case is the exchange-coupled metal cluster. Accordingly, single crystals of known structure should be used whenever possible. Their spectra can then be recorded with the electric vector ($\vec{E}$) of light parallel to the extinction directions of the crystal and then transformed to molecular axes. This is important, for the Tanabe mechanism is very restrictive, not only as regards spin-selection rules, but also with respect to symmetry-selection rules. The latter are based on the symmetry of the wavefunctions of the pair of ions in

the coupled dimer. Since possible differences in polarization behavior are expected depending on the intensity mechanism (single-ion or exchange), the observed polarizations can offer information about which mechanism is operative in giving the band its intensity. To obtain as much information as possible about exchange interactions from this technique, the various polarized spectra should be recorded as a function of temperature down to the lowest temperature available.

An example is the spectrum of basic rhodo perchlorate, $[(NH_3)_5Cr\text{-}OCr(NH_3)_5](ClO_4)_4$, shown in Fig. 9. Several features are noteworthy. (a) The band $\sim 17\,000$ cm^{-1} is not particularly sensitive either to polarization or to temperature. (b) The bands between 25 000 and 30 000 cm^{-1} are very intense and are almost totally polarized. They appear when $\vec{E}$ of light is parallel to z, the Cr–O–Cr axis. The lower band $\sim 25\,000$ cm^{-1} is a cold band, whereas the $\sim 27\,000$ cm^{-1} band, which completely disappears at 8 K, is a hot band. (c) The weak sharp band at 14 300 cm^{-1} is also a z-polarized hot band. As will be shown in Section D (iii), the knowledge of both the polarization and the temperature dependence of the near-UV bands was essential for their assignment.

Another example can be found in the spectrum of the mineral vivianite, $Fe_3(PO_4)_2 \cdot 8H_2O$ [63]. Several band systems in the visible part of the spectrum are completely polarized and extremely temperature sensitive. Figure 12 shows, as an example, the temperature dependence of a band system centered at $\sim 26\,500$ cm^{-1}, which is completely polarized along the crystal c axis. This complete polarization points to an exchange intensity mechanism, which is confirmed by their being hot bands. The measured temperature dependence was used to derive the value $2J = 5$ cm^{-1} for the ferromagnetic dimers in this material. See also Section D (v) for a more detailed discussion.

(ii) High resolution luminescence and excitation spectroscopy

All the trivalent lanthanide ions exhibit sharp line luminescence. In contrast, transition metal ions show luminescence only under very special circumstances, and the luminescence almost invariably takes place from the lowest energy excited state. This difference in behavior is due to the stronger electron–phonon coupling in the latter, which favors non-radiative relaxation processes. Among $3d$ complexes, which are of primary interest here, the $^2E \rightarrow {}^4A_2$ transition of Cr^{3+} is by far the best known and most intensively studied. As will be shown, high resolution luminescence and excitation spectroscopy are very powerful techniques for the study of exchange effects in Cr^{3+} clusters.

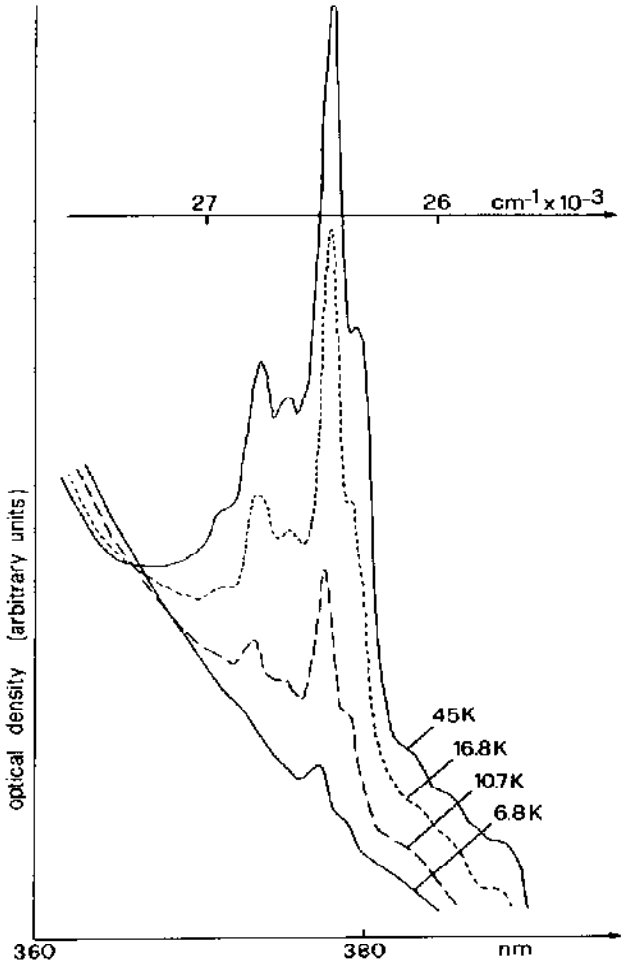

Fig. 12. Temperature dependence of the completely $\vec{E} \| c$ polarized 26500 cm^{-1} band system in vivianite, $Fe_3(PO_4)_2 \cdot 8H_2O$ [63]. (Reprinted with permission from Inorganic Chemistry. Copyright 1983 American Chemical Society.)

In a luminescence spectrum the sample is excited, either by broad-band or laser excitation. Excited transition metal centers then relax non-radiatively within 10^{-10} s to the lowest excited state, from which luminescence may be observed. A monochromator is usually used to disperse the luminescence. Information about the lifetime of the emitting state can be obtained by pulsed excitation and recording the time dependence of the luminescence intensity (see Section C (iv)).

In a luminescence excitation spectrum the intensity of a luminescence band is recorded as a function of the excitation wavelength. Tunable dye lasers are particularly useful light sources for high resolution excitation spectroscopy. In the absence of excitation energy transfer, the excitation spectrum corresponds to the absorption spectrum of the luminescent species.

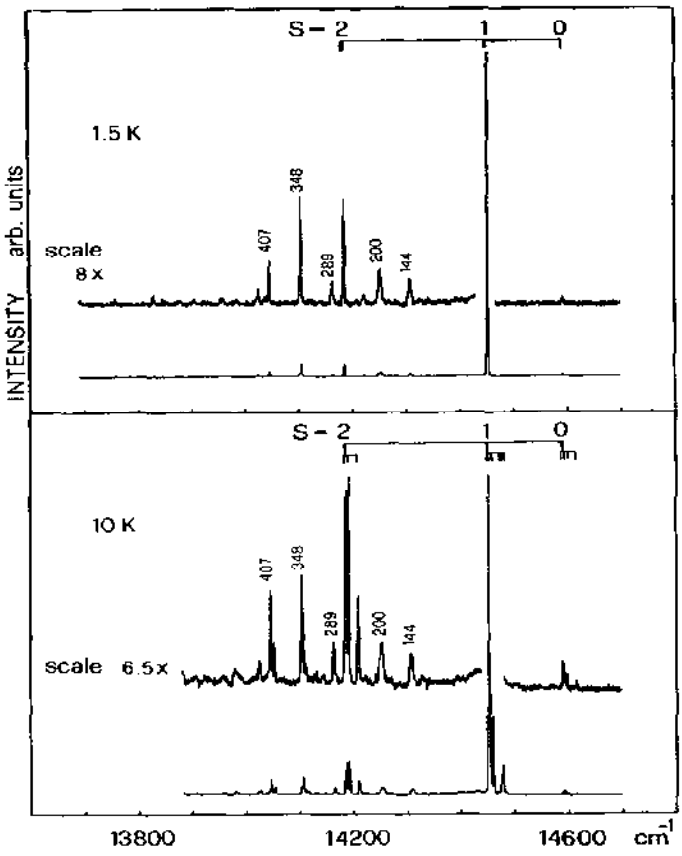

Fig. 13. Unpolarized luminescence spectra of {triol}$(ClO_4)_3$ at 1.5 K and 10 K. Pronounced vibrational sidebands are denoted with their energy shift from the strongest luminescence line. The purely electronic transitions are assigned to the dimer spin levels in the electronic ground state [4]. (Reprinted with permission from Molecular Physics.)

For transitions with very low oscillator strengths it may be superior to absorption spectroscopy because of its higher sensitivity. It is also useful for studying samples with more than one spectroscopically active center (see Section C (iii)), and for the study of excitation energy transfer. (Many aspects of the luminescence of inorganic solids are discussed in ref. 64.)

An example can be seen in Fig. 13 which shows the high resolution luminescence spectrum of {triol}$(ClO_4)_3$ [4]. At 1.5 K the spectrum shows exceedingly sharp lines with widths less than 1 cm^{-1}. This allows a very accurate determination of the exchange-energy splitting in the ground state and, in turn, the exchange parameters, $2J = -128 \pm 0.6$ cm^{-1} and $j = 1.6 \pm 0.5$ cm^{-1}. This is probably the most accurate ground state exchange splitting yet reported. Even the zero-field splitting of the $S = 1$ pair state (-2.25 ± 0.1 cm^{-1}) could be resolved and its sign determined from Zeeman

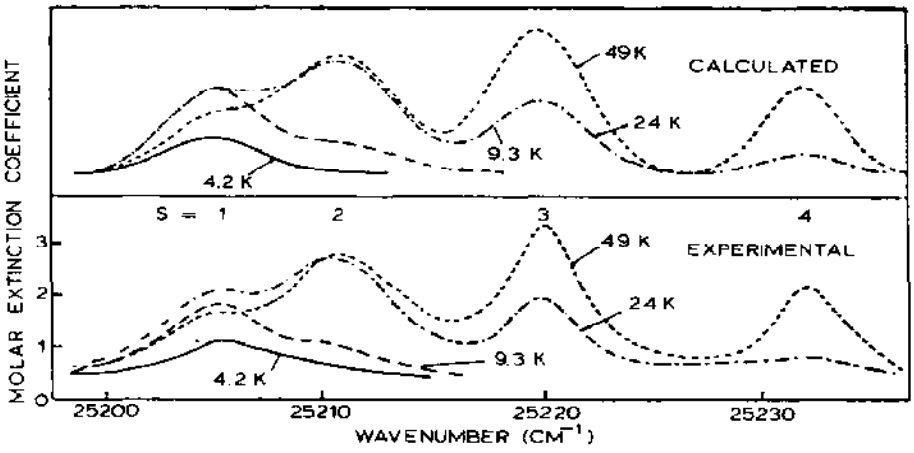

Fig. 14. High resolution luminescence excitation spectrum of the ${}^6A_1{}^6A_1 \rightarrow {}^4A_1{}^6A_1$ transition of Mn^{2+} pairs in $KMgF_3$. The calculated spectra are based on the mechanism in eqn. (7) with parameters $2J_{ex} = -10.6\ cm^{-1}$ and $2J = -7.5\ cm^{-1}$ for the excited state and ground state respectively. The ordinate is in ϵ per pair [27]. (Reprinted with permission from Molecular Physics.)

luminescence experiments. Further aspects of the spectroscopy of $\{triol\}^{3+}$ are discussed in Sections C (v), C (vi) and D (iii).

A second example is seen in Fig. 14, which shows the luminescence excitation spectrum of Mn^{2+} pairs in $KMgF_3$ in the region of ${}^4A_1$ single excitations [27]. The optical density of these transitions in absorption is so low that they are not observable. Sensitivity is increased by orders of magnitude in the excitation spectrum by monitoring the ${}^4T_1 \rightarrow {}^6A_1$ luminescence. The spectra are shown at various temperatures, and it is clear that all bands decrease in size as the temperature approaches 0 K. A $2J$ value of $-7.5\ cm^{-1}$ was derived for the ground state of the pair from the measured temperature dependence. The ${}^6A_1 \rightarrow {}^4A_1$ excitations of Mn^{2+} are pure spin flips, and for such pair excitations the theoretical model of Tanabe and coworkers [10,62,65] for both energy splittings and intensity enhancement is expected to be most successful. Indeed, the four observed $\Delta S = 0$ lines form a Landé energy pattern and their relative intensities exactly correspond to the theoretical ratio (after correction for Boltzmann populations) of 7 : 30 : 63 : 75 for the $S = 1, 2, 3, 4$ transitions. This can be seen in Fig. 14, which shows both the calculated and experimental spectra.

(iii) Site-selective spectroscopy and luminescence line narrowing

The compound $\{rhodo\}Cl_5 \cdot H_2O$ [6] provides a good example of the application of site-selective dye laser spectroscopy. Luminescence in this

complex will occur from the lowest excited pair level ($^5B_1$ in C_{2v} notation) to the four ground state levels, $^1A_1$, $^3B_2$, $^5A_1$ and $^7B_2$ (see Fig. 7(a)). When the crystal is irradiated with an Ar^+ ion laser (514.5 nm, 19431 cm^{-1}) at 1.5 K, at least six purely electronic luminescence lines are seen. This is due to two overlapping sets from two crystallographically inequivalent chromophores, A and B. If the sample is irradiated at 1.5 K with light which corresponds to the $^1A_1 \rightarrow {}^3A_2$ pair transition of site A (14862 cm^{-1}), luminescence will occur only from molecules on site A, while molecules on site B will be unaffected. The spectrum shows the expected four lines, the most intense corresponding to the allowed $^5B_1 \rightarrow {}^5A_1$ transition. When light of energy 14821 cm^{-1} is used, only the $^1A_1 \rightarrow {}^3A_2$ transition of molecules on site B is excited and another unique luminescence spectrum of four electronic lines is seen. Figure 7(a) shows the two site-selected pair spectra.

It will be noted that in addition to separating the two spectra this technique results in considerably sharper spectra. These sharp lines allow a very precise determination of the values of the exchange parameters in the ground state. For both of the principal sites A and B the parameters $2J = -30.6$ cm^{-1} and $j = 0.3$ cm^{-1} were obtained. It was also possible by selective excitation to determine the exchange-splitting pattern of minority sites, which are related to crystal defects and account for less than 1% of all the dimers in the crystal. For one such site, $2J = -32.2$ cm^{-1} and $j = 0.5$ cm^{-1}, values significantly different from those of the majority sites. The biquadratic exchange parameter j is, as expected, about 1% of $|2J|$ for the regular sites, but may be considerably larger for distorted sites, probably as a result of exchange-striction effects. We may note again the extremely high selectivity of the technique, in contrast to bulk techniques such as magnetic susceptibility and heat capacity measurements which have no selectivity. Furthermore, the presence of two crystallographically inequivalent dimer sites in this material has not been detected by X-ray diffraction.

The complete separation of the two spectra at 1.5 K means that any transfer of excitation energy between sites A and B during the lifetime of the excited state is negligible. When the temperature is raised, for example to 34 K, the situation changes and selective excitation of site A results in a mixed luminescence spectrum approaching that shown at the top of Fig. 7(a). This means that even at 34 K, excitation energy is transferred non-radiatively from site A to B (see Section C (iv)).

Site selection can also be accomplished by recording the intensity of a sharp luminescence line as a function of excitation energy. For {rhodo}$Cl_5 \cdot H_2O$ such experiments were carried out with the $^5B_1 \rightarrow {}^5A_1$ luminescence lines of sites A and B, and yielded the pure excitation spectra of the two sites at 1.5 K. The superposition of sites A and B present in the absorption spectrum could thus be resolved. At higher temperature, where excitation

energy transfer sets in, the excitation spectrum of the site B luminescence was found to be a superposition of site A and site B excitations.

The same techniques have been applied to the $\{triol\}^{3+}$ related compound, $[(L)Cr(OH)_3Cr(L)]Br_3 \cdot 2H_2O$ (L = 1,5,9-triazacyclododecane) [66], which also possesses two inequivalent crystallographic sites. The values of $2J$ for the two sites are -99.0 and -105.0 cm^{-1}. They are significantly different as a result of the different geometries of the two dimers. Again, this is a result which could not be obtained by non-spectroscopic techniques.

Closely related to site-selective spectroscopy is the technique of luminescence line narrowing. In a crystal of any substance there are structural dislocations, strains and unintended impurities. All of these can lead to a distribution of sites which differ very slightly from one another. As might be expected, spectral absorption and emission lines will mirror this distribution, and will not be infinitely sharp, but will be broadened over a range of values. This inhomogeneous line broadening can be partially overcome by the technique of luminescence line narrowing. The technique is well established in the spectroscopy of transition metal and lanthanide centers in glasses [67]. These are systems with extremely large inhomogeneities, in which the method can be used to its greatest advantage. The principal aim in these studies is the exact determination of the homogeneous line widths and the underlying interactions, as well as an understanding of energy-transfer processes.

This technique has only recently been applied to molecular complexes. An example is the study of $[LCr(OH)_2(SO_4)CrL](S_2O_6) \cdot 3H_2O$ (L = bispicam = *N*,*N*′-bis(2-pyridylmethyl)amine) [68]. The compound has one bridging sulfate and two bridging hydroxo groups [69]. Like other Cr^{3+} dimers, its ground state consists of four spin levels with $S = 0, 1, 2, 3$. The lowest singly excited dimer state is $^2E^4A_2$ with an $S^* = 2$ emitting level [20]. When the compound is excited with the 520.8 nm (19196 cm^{-1}) Kr^+ ion laser line, the four dimer transitions are unresolved in the luminescence spectrum even at 1.5 K (Fig. 15, trace (a)) [68]. This can be understood by considering Fig. 16 [68]. The energy of the emitting level, $S^* = 2$, varies over a finite range, $\Delta\nu_i$. The luminescence transitions to the ground state levels will vary somewhat in energy depending on the site. This causes the lines to be broad and to overlap. $\Delta\nu_i$ is particularly large in this compound, i.e. the inhomogeneous line broadening is very pronounced.

The $S = 0 \rightarrow S^* = 2$ absorption at 1.5 K is centered at 13958 cm^{-1} and, being doubly spin forbidden, is extremely weak. Light of this energy can be obtained with a dye laser and used as the excitation source for the line-narrowing experiments. Only those molecules having their $S^* = 2$ level at the laser energy will be excited. Others at slightly different sites will not be excited. In the absence of energy transfer, the transitions to the $S = 3, 2, 1$

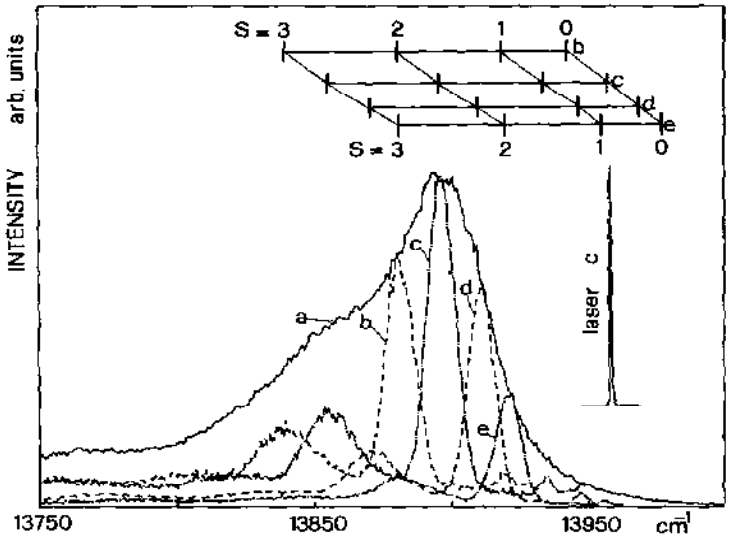

Fig. 15. Luminescence spectra of $[LCr(OH)_2(SO_4)CrL]S_2O_6 \cdot 3H_2O$ (L = bispicam) (see text) at 1.5 K for several excitation energies: (a) 19196 cm^{-1} (non-selective); (b) 13944.0 cm^{-1}; (c) 13958.3 cm^{-1}; (d) 13969.4 cm^{-1}; (e) 13977.4 cm^{-1}. The shape of the laser line used for excitation of spectrum (c) is shown. Spin quantum numbers of the final ground state levels are shown for spectra (b)–(e) [68]. (Reprinted with permission from Chemical Physics Letters.)

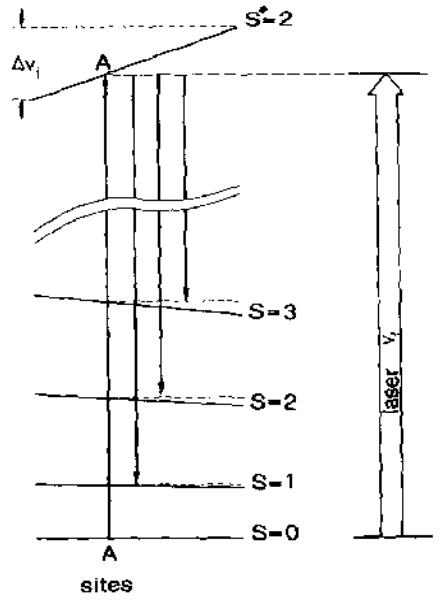

Fig. 16. Schematic representation of luminescence line-narrowing in a Cr^{3+} dimer. The slopes of the various levels represent the variation in their energies as a function of the site. $\Delta\nu_i$ denotes the inhomogeneous broadening of the $S = 0 \rightarrow S^* = 2$ transition. Using the laser frequency ν_1, the subset A is excited [68]. (Reprinted with permission from Chemical Physics Letters.)

ground levels will then be much sharper and will be separated in the spectrum. This is shown schematically in Fig. 16 by the arrows connecting the dotted horizontal lines. By tuning the dye laser through the profile of the absorption line, different subsets of the inhomogeneous distribution are selectively excited (see Fig. 15). At 1.5 K the narrowed luminescence peaks can be assigned as dimer transitions to the $S = 1, 2, 3$ ground state levels and exchange parameters can be determined. In this compound the exchange splitting was found to vary quite strongly within the inhomogeneous distribution. $2J$ and j values ranging from -15.6 and 1.2 cm^{-1} to -14.4 and 1.0 cm^{-1} were found.

It is interesting to note that at 1.5 K the luminescence lines are not as narrow as the exciting laser line, since even at 1.5 K there is some interdimer energy transfer which broadens the lines. At 10 K this is so efficient that no narrowing is observed any more. This is the result of spectral energy transfer between the subsets of the site distribution, which obviously occurs with a very low activation energy. The exchange splittings obtained in this spectroscopic study are at variance with the conclusions from magnetochemical measurements. Our confidence that the spectroscopic values are correct is based on the fact that the energy differences can be directly observed in this experiment, whereas in a magnetochemical study they can only be deduced by fitting a theoretical model to the data.

Site-selective spectroscopy is an indispensable tool for the study of Cr^{3+} pairs in a crystal such as ruby. The superpositions in the spectrum can be partially resolved into the many constituent chromophores or luminophores (see Section D (i)).

(iv) Time-resolved spectroscopy

Time-resolved spectroscopy (TRS) is closely related to site-selective spectroscopy. It is important when there is more than one crystallographically inequivalent luminescent center in the material. The inequivalent centers may have different luminescence lifetimes, and discrimination between the centers can be made by the use of TRS, if the difference in lifetimes is great enough. The condition for this application is that there be negligible excitation energy transfer between the inequivalent sites.

Another important related aspect is that of emission rise and decay times. Radiative decay times are inversely proportional to the oscillator strength of the luminescence transition. A consequence is that in exchange-coupled systems, in which there can be exchange enhancement of the intensity of spin-forbidden transitions, there can also be shorter radiative lifetimes. An example of this has been given in Section B (v) for the $^1E \rightarrow {}^3T_1$ emission of Ti^{2+} in $MgCl_2$ and $MnCl_2$. In the exchange-coupled system, $MnCl_2 : Ti^{2+}$,

the emission lifetime is 327 μs (15 K), while it is considerably longer, 125 ms (13 K), for $MgCl_2 : Ti^{2+}$ [48]. Another example is the emission spectrum of pink ruby, which is basically the $^2E \rightarrow {}^4A_2$ transition of Cr^{3+}. The so-called N lines, which are due to exchange-coupled Cr^{3+} pairs, have shorter radiative lifetimes than the R lines, which are due to single Cr^{3+} ions.

In most molecular Cr^{3+} dimers, like the singly, doubly and triply hydroxo-bridged complexes, the emission lifetimes are non-radiative down to the lowest temperatures owing to the large number of N–H or O–H bonds with high energy stretching vibrations which are involved in the non-radiative relaxation process. In $[(H_2O)_4Cr(OH)_2Cr(H_2O)_4]^{4+}$ this is so dominant that no luminescence could be observed down to 2 K [70].

When transfer of excitation does take place, then TRS and decay-time measurements are most useful. An example is the spectrum of {rhodo}$Cl_5 \cdot H_2O$ shown in Fig. 17 [6]. At 35 K the center of the site A absorption band at 14862 cm^{-1} was excited with a pulsed laser. As noted above, at this temperature there will be considerable energy transfer from site A to B. The rate is monitored by recording the emission from both A and B sites at varying times after the initial 150 ns pulse. The spectra corresponding to three delay times (0.5–5.2 μs) are shown in Fig. 17(a). Figure 17(b) shows the intensity of emission from the two sites at 54 K as a function of time after the initial site A excitation. The rise in site B emission parallels the fall in site A emission. From these data, it is possible to derive excitation energy transfer rates. In Section C (iii) the A $\rightarrow$ B transfer process in {rhodo}$Cl_5 \cdot H_2O$ was shown to be thermally activated. At 80 K and at 30 K the rate is of the order of 10^6 s^{-1} and 10^5 s^{-1} respectively.

A simple picture to account for this behavior is the following. In $\{rhodo\}^{5+}$ the transition from the lowest level of the ground state ($S = 0$) to the lowest level of the first excited state ($S^* = 2$) is doubly spin forbidden and therefore extremely weak. As a consequence, excitation energy transfer involving this transition in an electric dipole–dipole process is extremely slow at 1.5 K. However, with the population of the $S = 2$ ground state level, a formally allowed transition occurs to the lowest emitting level, which is then used in a phonon-assisted non-radiative electric dipole–dipole energy-transfer process. This leads to highly increased transfer rates at higher temperatures, proportional to the $S = 2$ ground state level population.

While non-radiative excitation energy transfer between molecules in a concentrated crystal is a very general phenomenon, the dimeric exchange-coupled nature of the constituent molecules here brings in a special aspect. Since dipole strength is needed for an electric dipole–dipole process, interdimer transfer is strongly inhibited at very low temperatures owing to the vanishing intensity of the transition from the lowest energy ground state to the lowest energy excited state level.

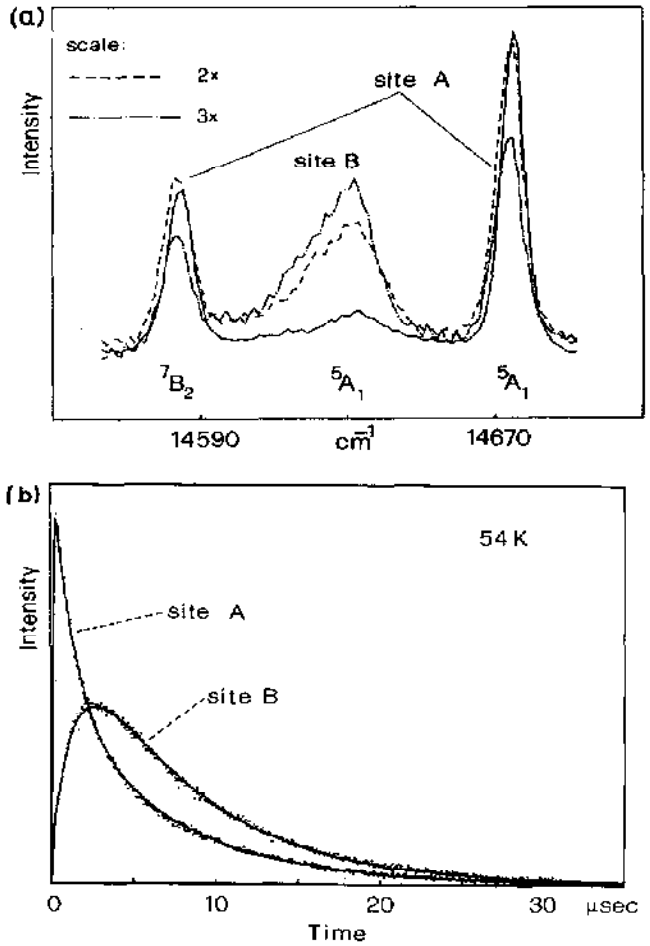

Fig. 17. (a) Time-resolved luminescence spectra of {rhodo}$Cl_5 \cdot H_2O$ for three delays at 35 K (pulsed selective excitation of site A at 14862 cm^{-1}): ———, 0.5 μs delay; — — —, 2.9 μs delay; ·–·–, 5.2 μs delay. (b) Time dependence of $^5B_1 \rightarrow {}^7B_2$ luminescence intensities at 54 K. Selective site A excitation at 14673 cm^{-1} ($^5A_1 \rightarrow {}^5B_1$), pulse width 150 ns, laser width 0.5 cm^{-1} [6]. (Reprinted with permission from Molecular Physics.)

(v) Zeeman, MCD and MCPL spectroscopy

These techniques allow a detailed characterization of the ground and excited state levels involved in an absorption or emission transition. Often g values for both states can be derived and the symmetry of the states determined.

Figure 18 shows the absorption spectra of the lowest energy excitations in {triol}$(ClO_4)_3$ at 1.5 K in magnetic fields ($H \perp c$) up to 5 T [4]. Besides the line splittings, which lead to an accurate determination of g values, the spectra show a redistribution of intensity in the lines with increasing

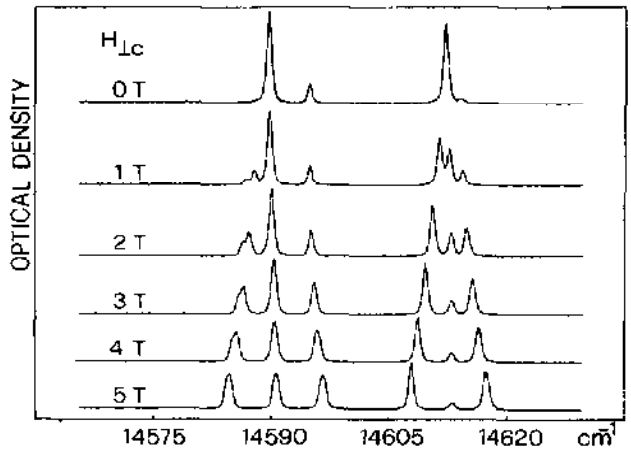

Fig. 18. Axial polarized absorption spectra of {triol}$(ClO_4)_3$ in magnetic fields ($H \perp c$) between 0 and 5 T for the lowest energy excitations at 1.5 K [4]. (Reprinted with permission from Molecular Physics.)

magnetic field as a result of the magnetic field's action on the wavefunctions. In the spectra one clearly sees the transition from a situation in which the principal axis of anisotropy is the trigonal (Cr–Cr) axis of the complex (zero field), to one in which the Zeeman effect is the dominant anisotropy. As the magnetic field ($H \perp c$) is increased, the system becomes quantized perpendicular to c.

A quantitative analysis of all the Zeeman data on this compound led to the g values of the spinors of the first $^3E''$ and $^3E'$ excited pair states shown in Fig. 19 [4]. These g values, which deviate strongly from those expected for a pure $^2E\,^4A_2$ state, were a very important clue in the interpretation of

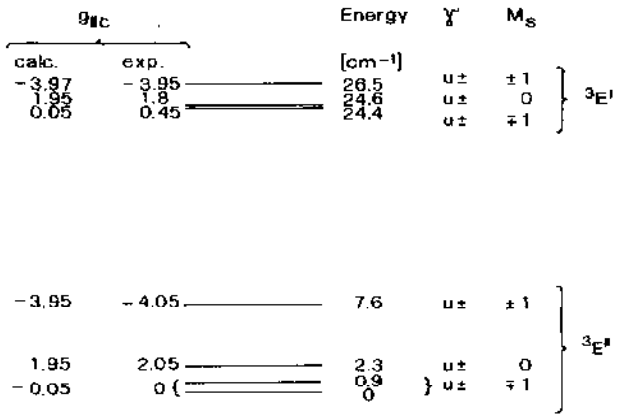

Fig. 19. Spinor levels $|^3\Gamma_\gamma M_s\rangle$ of the two lowest energy excited multiplets $^3E''$ and $^3E'$ of {triol}$(ClO_4)_3$. Energies, assignments, calculated and experimental $g_{\parallel c}$ values are given. Ordinate scale: add 14589.5 cm^{-1} [4]. (Reprinted with permission from Molecular Physics.)

the excited pair states. They clearly show a strong mixture of $^2E^4A_2$ and $^2T_1^4A_2$ pair functions. A calculation, the result of which is indicated in Fig. 19, revealed that this mixing did not primarily occur as a result of the strong trigonal ligand-field component, as might have been expected, but as a result of exchange interactions.

When absorption or emission lines are not as sharp as in $\{triol\}(ClO_4)_3$, MCD rather than Zeeman spectroscopy is the technique to be used to derive information about the magnetic moments of the pair states. This was particularly important in the studies of $Cs_3Cr_2Cl_9$ [71] and $Cs_3Cr_2Br_9$ [25] (cf. Section D (ii)). MCD is important also in the study of active Cu^{2+} and Fe^{3+} centers in proteins. In these systems it is a convenient and selective probe of the ground state magnetic properties. Antiferromagnetically coupled dimers can be recognized by the absence of C terms in the MCD spectrum at low temperatures.

(vi) Pressure dependence of exchange effects

Since the exchange coupling is a sensitive function of the geometry of the bridged system, it is not surprising that high pressure affects the coupling and alters the value of J. Recently a study appeared on the effect of pressures up to 40 kbar on the low temperature spectra of $\{rhodo\}Cl_5 \cdot H_2O$, and of $\{triol\}(ClO_4)_3$ [72]. Figure 20 shows the luminescence spectra of the latter compound at 14 K and at several pressures. The pressures were calibrated using the shift of the ruby luminescence line, R_1, since the pressure effects on the latter are well documented [73]. The R_1 line is shown on two of the spectra. The observed energy shifts with pressure in $\{triol\}(ClO_4)_3$ are quite dramatic, up to several hundred wavenumbers at 40 kbar, i.e. about two orders of magnitude larger than those of the ruby R_1 line. The observed shifts are the result of changes in the intraionic electron-repulsion parameters and the exchange parameters. The full data analysis led to the following results. As was already shown in Section C (ii) (Fig. 13), $2J = -128$ cm^{-1} and $j = 1.6$ cm^{-1} at ambient pressure [4]. It was found that the dependence of J on pressure is linear in the pressure range studied and can be expressed by the equation $|J(P)| = |J_0| + (0.7 \pm 0.1$ cm^{-1} kbar$^{-1}) \cdot P$. The biquadratic term was essentially constant within experimental accuracy.

For $\{rhodo\}Cl_5 \cdot H_2O$ the following pressure dependence was obtained: $|J(P)| = |J_0| + (0.15 \pm 0.02$ cm^{-1} kbar$)^{-1} \cdot P$. Considering the $2J$ value of -30.4 cm^{-1} at ambient pressure, the relative pressure dependence is practically the same as in $\{triol\}(ClO_4)_3$.

In order to correlate these changes in the magnetic coupling with structural changes under hydrostatic pressure, these latter were estimated from

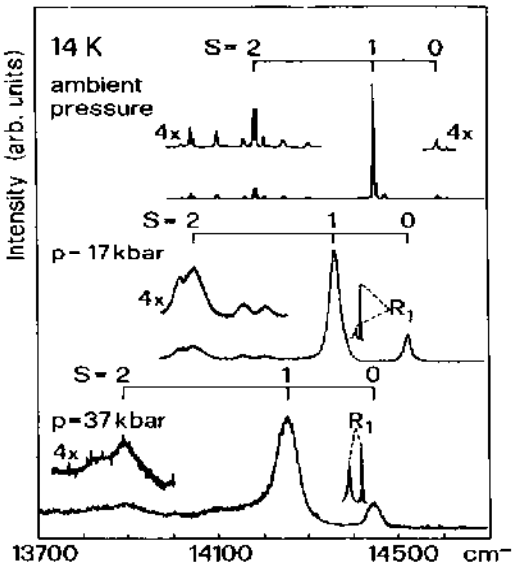

Fig. 20. 14 K luminescence spectrum of $\{triol\}(ClO_4)_3$ at various pressures. The ruby R_1 lines of the internal pressure standard and the sapphire anvil are shown for the 17 and 37 kbar spectra. Spin quantum numbers of the dimer ground state levels are indicated. Excitation: 476.2 nm Kr^+ ion laser line; ~10 mW [72]. (Reprinted with permission from Journal of Chemical Physics.)

the shifts of the spin-allowed $^4A_2 \rightarrow {}^4T_2$ absorption band in the same pressure range. Assuming isotropic contraction under pressure the relative volume dependence $(-(V/J)\,dJ/dV)$ was found to be 10.9 and 16.4 for the two compounds $\{triol\}(ClO_4)_3$ and $\{rhodo\}Cl_5 \cdot H_2O$ respectively. The volume dependence of J was then calculated by an Extended Hückel MO calculation, and it was found that the calculation underestimates the experimental effect by a factor of three, but that the significantly higher volume dependence of the acid rhodo complex was well reproduced.

D. SPECIFIC SYSTEMS

(i) Pair spectra in diamagnetic host lattices

(a) Oxide lattices

The diamagnetic host lattices that have been most extensively used to study exchange interactions are metal oxides, and of these Al_2O_3 is among the most important. A large body of work has been carried out on ruby, which is Al_2O_3 doped with Cr^{3+}. Schawlow et al. [3] were the first to suggest that the many sharp lines in absorption and emission which are found as "satellites" to the R lines in ruby are due to pairs of exchange-coupled Cr^{3+} ions (see Fig. 3).

The spectrum of ruby is very complex, since there is considerable exchange interaction between Cr^{3+} ions up to the fourth neighbors and, as a result, considerable overlap of spectral lines belonging to different chromophores and luminophores. Most of the important early references to ruby are cited by Naito [12], who himself gives a theoretical treatment of the various couplings out to the fourth neighbor pair. The complexities of the spectra have been in part overcome by the use of site-selective spectroscopy and time-resolved spectroscopy. Despite the application of these refined techniques, however, even the first nearest-neighbor ($1nn$) Cr^{3+} pairs of ruby are not completely understood, as is evident from the following discussion.

A very extensive spectroscopic study of the ($1nn$) Cr^{3+} pairs in ruby was reported in 1974 by van der Ziel [36]. This pair has trigonal symmetry and consists of two face-sharing CrO_6 octahedra. The principal results are as follows. (a) The ground state exchange parameters in eqn. (3) are $2J = -54$ cm^{-1} and $j = 8.7$ cm^{-1}. (b) The pair transitions obtain their intensity mainly from the single-ion mechanism. The exchange-induced intensity, which often dominates the pair spectrum, is considered to be weak here as a result of the D_{3h} pair symmetry. (c) Double excitations are observed at nearly twice the energy of the $^4A_2 \rightarrow {}^2E$ transitions. Their σ polarization agrees with that expected for a Tanabe mechanism. A few years later (1976) Platz and Heber [74] reported another detailed spectroscopic study of the ($1nn$) Cr^{3+} pairs in ruby. On the basis of the assignment of a number of lines in the excitation spectra, they calculate the exchange parameters as $2J = -115$ cm^{-1} and $j = 0.7$ cm^{-1}. Finally, in 1979 Ferguson and van Oosterhout [75] identified two new emission lines which they identified with the ($1nn$) Cr^{3+} pair. This led to their evaluation of the exchange parameters as $2J = -112$ cm^{-1} and $j = 2.6$ cm^{-1}.

Several other reports on ruby that are worthy of note have appeared. Excitation spectroscopy was used by Ferguson and van Oosterhout [76] to measure the Zeeman splitting of the $^4A_2{}^4A_2 \rightarrow {}^2E{}^4A_2$ transitions in the ($1nn$) Cr^{3+} pair in ruby. They present evidence for a large trigonal field splitting. The effects of thermal pulses on the luminescence of ruby at 1.8 K have been reported by Basun et al. [77]. Their data bear on the energy structure and relaxation in distant Cr^{3+} pairs (fifth and higher order). Mitrofanov et al. [78] have studied the far-IR absorption lines due to transitions between the ground state energy levels of Cr^{3+} pairs in ruby. The pressure shift of several near-neighbor Cr^{3+} pair emission lines in ruby have been measured by Williams and Jeanloz [79]. They found that all near-neighbor pair lines shift to lower energy with increasing pressure. Heber and Platz [80] have studied the influence of uniaxial pressure along the C_3 axis on the value of the exchange parameters for the first and second nearest Cr^{3+} pairs in ruby. Monteil and Duval [81] have researched the energy transfer rates between

Cr^{3+} single ions and Cr^{3+} pairs in ruby by means of chronospectroscopy. In the concentration range 0.1%–1.4% they found that the process is mainly by an exchange mechanism. Wasiela and coworkers have studied the luminescence [82] and the energy transfer [83] in gallium-doped ruby. Time-resolved fluorescence line-narrowing measurements enabled them to determine the energy levels for a pair of loosely bound chromium ions. Imbusch [84] has recently reviewed the excitation energy transfer processes in ruby, in which Cr^{3+} pairs play an important role. The literature on ruby is not completely covered in this short summary.

Studies of other metals in Al_2O_3 have appeared. V^{3+} pairs in Al_2O_3 have been investigated by Hasan et al. [85] using phonon spectroscopy. Ferguson and Fielding [86] have measured the absorption spectra of natural and synthetic yellow sapphires, which are basically Al_2O_3 containing Fe^{3+} and other impurity ions. They have shown that the absorption in natural yellow sapphites is due to single Fe^{3+} ions and Fe^{3+}–O^{2-}–Fe^{3+} pairs. Two bands were found to decrease in size as the temperature is lowered, and from the temperature dependence of one of them ($\sim 22\,000$ cm^{-1}) they conclude that one pair is mainly involved, probably the fourth nearest-neighbor pair; for this $2J = -25$ cm^{-1} and $j = 0.75$ cm^{-1}. Blue and green natural sapphires contain other bands which can be associated with Ti^{4+}–O^{2-}–Fe^{2+} and Fe^{2+}–O^{2-}–Fe^{3+}. The researchers also observed four double excitations at high energy in the spectra of natural yellow sapphires.

Van der Ziel has studied the absorption and emission spectra of nearest-neighbor Cr^{3+} pairs in $LaAlO_3$ [16]. The structure of the host is simpler than ruby, and this results in the predominance of only one type of pair spectrum, namely that between first nearest neighbors. The spectra yield ground state exchange parameters, $2J = -66.6$ cm^{-1} and $j = 0.76$ cm^{-1}. Exchange parameters for the $^2E^4A_2$ excited state were also derived. The author also observed $^2E^2E$ double excitations [16,87]. An extended treatment of the non-radiative transfer of optical excitation energy from Cr^{3+} single ions to the first nearest Cr^{3+} pairs in this system has appeared [88]. Time-resolved laser spectroscopy was used, and the luminescence due to single ions and pairs was monitored. An exchange mechanism was found to be responsible for the process. A theoretical treatment of Cr^{3+} pairs in $LaAlO_3$ has been reported [89].

Van der Ziel [37] has also reported the spectra of two types of Cr^{3+} pairs in the orthorhombic $YAlO_3$ lattice. The exchange parameters are (a) $2J = -24.7$ cm^{-1} and $j = 0.66$ cm^{-1} and (b) $2J = -26.2$ cm^{-1} and $j = 0.91$ cm^{-1} for the two sets. Uniaxial stress experiments were used to identify the two sets of pairs in the crystal. Double excitations were observed at about twice the energy of the ^2E band. A similar study has been reported for Cr^{3+} pairs in $Y_3Al_5O_{12}$ [90].

The emission, absorption and luminescence excitation spectra of Cr^{3+} pairs in the spinel, $ZnGa_2O_4$, have been reported by van Gorkom et al. [18]. The ground state exchange parameters are $2J = -22.2 \pm 0.5$ cm^{-1} and $j = 1.7 \pm 0.3$ cm^{-1}. They also calculated the orbital excited-state exchange parameters. Van Gorkom [91] has also studied the optical spectra of doubly excited pairs ($^4A_2{}^4A_2 \rightarrow {}^2E{}^2E$) in this system. He noted especially that in order to calculate the energy level diagram of the doubly excited state, some of the orbital exchange parameters, $J_{ai\,bj}$, had to have different values from those of the ground state ($^4A_2{}^4A_2$) or of the singly excited state ($^2E{}^4A_2$).

The absorption and luminescence spectra of the Cr^{3+}-doped spinels, $ZnAl_2O_4$ and $MgAl_2O_4$, have been studied by Wood et al. [92]. While their spectra showed evidence of pair formation, they reported no exchange parameters. The luminescence spectra of these two spinels have been further investigated by Derkosch et al. [93]. The reported ground state exchange parameters are $2J = -40.9$ cm^{-1} and $j = -1.5$ cm^{-1} for the zinc salt and $2J = -45.6$ cm^{-1} and $j = -2.0$ cm^{-1} for the magnesium salt. Another determination of the ground state exchange parameters for nearest-neighbor Cr^{3+} pairs in $MgAl_2O_4$ from emission and luminescence excitation spectra yielded values, $2J = -29 \pm 3$ cm^{-1} and $j = 3 \pm 2$ cm^{-1} [94]. The fact that different parameter values were obtained using the same techniques on the same system, Cr^{3+} pairs in $MgAl_2O_4$, clearly demonstrates that there is some ambiguity in the assignment of luminescence and absorption lines. The problem is similar to that encountered in ruby, even though only first nearest-neighbor pairs significantly contribute to the spectrum in the spinel lattice. There is the dominant and overlapping spectrum of single Cr^{3+} ions, which is so much more intense than the pair spectrum that it is quite easy to mistake a weak vibrational sideband of the single ion for a pair band. The negative sign of the biquadratic parameter in ref. 93 is unusual and suspicious.

A detailed report of the spectra of the laser material alexandrite ($BeAl_2O_4 : Cr^{3+}$) has appeared recently [95]. In the crystal the Cr^{3+} ions exist in two different sites, one on a mirror plane, the other at an inversion center. Site-selection luminescence spectroscopy at low temperature on the Cr^{3+} ions in inversion sites enabled the researchers to identify six types of exchange-coupled pairs of Cr^{3+} ions in the lattice. Of these, two are reported to be ferromagnetically coupled and four antiferromagnetically coupled. The researchers did not identify the exact lattice sites involved in the six different Cr^{3+} pairs.

A particular subgroup of Cr^{3+}–Cr^{3+} interactions are the 90° interactions, such as those which occur in spinels. MacCraith et al. [96] have studied Cr^{3+} substituted in $LiGa_5O_8$ which has an inverse spinel structure. The variation in the $^2E \leftrightarrow {}^4A_2$ luminescence and absorption with temper-

ature, as well as the variations in the spectra as the chromium concentration varied from $< 0.001\%$ to 1% enabled them to derive the exchange parameters $2J = -35.8\ cm^{-1}$ and $j = 1.4\ cm^{-1}$. Their report compares these values with those reported for Cr^{3+} substituted in similar lattices. Gutowski [17] also studied the same system by ESR and optical spectroscopy and reported the exchange parameters $2J = -27 \pm 1\ cm^{-1}$ and $j = 0.6 \pm 1.3\ cm^{-1}$. The orbital exchange parameters for the $^2E^4A_2$ excited state were also determined.

McDonagh and Henderson [97] have studied the luminescence of Cr^{3+} ions in MgO. Selective excitation revealed two types of Cr^{3+} pairs. In each the two Cr^{3+} are separated by an Mg^{2+} vacancy (V) needed to obtain overall charge balance in the crystal. In one type the Cr–V–Cr angle is 180°, while in the other it is 90°. The exchange is reported to be ferromagnetic in the $^2E^4A_2$ excited state, and antiferromagnetic in the ground state with exchange parameters $2J = -1.5 \pm 0.1\ cm^{-1}$ for the bent and $2J = -(4 \pm 1) \times 10^{-3}\ cm^{-1}$ for the linear chromium couple. The energy transfer between Cr^{3+} ions from cubic to tetragonal centers in this system has also been reported [98].

The NIR luminescence of Ni^{2+} and Ni^{2+} pairs in MgO has been reported [99]. Effective energy transfer from isolated ions to the pairs was observed at temperatures below 40 K. Ni^{2+}–Ni^{2+} exchange has also been studied in $NiWO_4$ and Ni^{2+}-doped $ZnWO_4$ [100].

Several Fe^{3+}-bearing minerals (monoclinic pyroxenes, amphiboles, micas etc.) have a broad, intense absorption band in the 13000–18000 cm^{-1} region, which is generally attributed to an $Fe^{2+} \rightarrow Fe^{3+}$ intervalence electron transfer. Bakhtin and Vinokurov [101] have proposed an alternative interpretation, namely, that this band is due to an electric dipole $^5T_2{}^6A_1 \rightarrow {}^5T_2{}^4T_2$ transition in an exchange-coupled Fe^{2+}–Fe^{3+} pair, accomplished through the excitation of the Fe^{3+} ion.

Smith [102] has studied the polarized absorption spectra of biotite and tourmaline in the NIR region. He noted a reduction in intensity of the bands between 9000 and 14000 cm^{-1} upon chemical reduction. He concludes that a definite assignment of these bands to normal *d–d* excitations, charge-transfer transitions, or exchange-enhanced *d–d* excitations is difficult. The situation is reminiscent of $[Fe_3O(Ac)_6]^+$, in which the first absorption band around 10000 cm^{-1}, assigned as a $^6A_1 \rightarrow {}^4T_1$ *d–d* transition, is enhanced three orders of magnitude by the proximity of close-lying charge-transfer transitions (see Section D (v)).

These absorption bands strongly contribute to the deep colors of these minerals, and because of their intensity, may more plausibly be interpreted in terms of electron transfer. Some of these bands show a drastic increase in intensity on cooling to 15 K. Examples can be found in the spectra of biotite

and tourmaline [103]. This highly unusual behavior may be the result of exchange interactions. In an Fe^{2+}–Fe^{3+} pair with both ions in a high spin electron configuration, there is exchange coupling between the two Fe ions. As a consequence of this coupling the intervalence electron transfer can be more or less strongly inhibited, depending on the total spin state of the dimer and thus on the temperature.

(b) Halide lattices

Next to oxide lattices the most common matrices used to study pair spectra have been halide lattices.

Some important earlier studies on Mn^{2+} pairs were carried out on the cubic perovskites, $KMnF_3$, $RbMnF_3$, and Mn^{2+} substituted in $KZnF_3$ [8,65]. Later work was carried out on Mn^{2+} substituted in $KMgF_3$ [27,34,104], as well as in $KZnF_3$ [104], and in $RbMgF_3$ [105]. Perhaps the most detailed study of Mn^{2+} pairs in a fluoride lattice is that of ref. 27, in which the $^6A_1{}^6A_1 \rightarrow {}^4A_1{}^6A_1$, $^4E^6A_1$ single excitations were investigated by the highly sensitive technique of excitation spectroscopy. This was discussed in Section C (ii).

The spectra of nearest-neighbor Ni^{2+} pairs in $KMgF_3$ [106,107] and in $KZnF_3$ [107] have been investigated, and the value of $2J$ for the antiferromagnetically coupled Ni^{2+} pairs in $KMgF_3$ is reported as -68 cm^{-1} [108]. The mechanism of concentration quenching of the $^1T_2 \rightarrow {}^3A_2$ luminescence of Ni^{2+} in $KZnF_3$ has been reported [109]. The researchers found that in crystals of higher than 0.59% Ni^{2+} concentration, decay was not exponential. This they attributed to non-radiative and resonant energy transfer between a pair of Ni^{2+} ions (cross relaxation). Although no visible spectra have been reported for V^{2+} pairs in $KMgF_3:V^{2+}$, a detailed ESR study of this mixed crystal has been reported [110].

Examples exist of the spectra of exchange-coupled pairs of two different paramagnetic ions in fluoride lattices. Mn^{2+}–Ni^{2+} pairs have been studied in $KZnF_3$ [13,62,111,112] and in $KMgF_3$ [111]. The ground state exchange parameter in $KZnF_3$ is $2J = -18$ cm^{-1} [62]. The theory of Mn^{2+}–Ni^{2+} pairs in $KZnF_3$ has been discussed by Mitrofanov et al. [89]. Ni^{2+}–Co^{2+} pairs in $KMgF_3$ have also been reported [108]. The emission lifetimes at 15 K for the Ni^{2+}–Co^{2+} pairs is 5 ms, as compared with 2 ms for Ni^{2+}–Ni^{2+} pairs. Mn^{2+}–Cu^{2+} pairs in $KZnF_3$ have also been investigated [113,114]. The reported value of the ground state exchange parameter is $2J = -130$ cm^{-1} [114]. The near-UV spectrum of Cu^{2+}–Mn^{2+} pairs in $KZnF_3$ [114] is noteworthy, since it contains a very unusual feature, a rather intense, broad band centered at $\sim 40\,000$ cm^{-1} and exhibiting a long progression in a mode of about 1290 ± 70 cm^{-1}, which is not further identified by the researchers. This band is not observed in crystals which are doped with only

Cu^{2+} or Mn^{2+}, and so it is likely due to Cu^{2+}–Mn^{2+} pairs. It is no doubt a charge-transfer band, but whether it should be assigned as an $Mn^{2+} \rightarrow Cu^{2+}$ or an $F^- \rightarrow Cu^{2+}$ electron transfer is not clear. It is known from studies of various Cu^{2+} and Mn^{2+} chloride compounds that the positions of $Cl^- \rightarrow Cu^{2+}$ electron-transfer bands can be strongly red shifted by the presence of neighboring Mn^{2+} ions in the lattice [115].

There exists a large number of halide compounds of stoichiometry RMX_3 which have the $CsNiCl_3$ structure (space group $P6_3/mmc$ (D_{6h}^4)) [11]. Among these are $CsMgCl_3$, $CsMgBr_3$ and $CsCdBr_3$, all of which have served as diamagnetic host lattices for paramagnetic $3d$ ions. The host lattice consists of parallel, infinite chains of face-sharing octahedra. Each M stands at the center of a slightly elongated, trigonally distorted octahedron of X atoms, and the M–M axis lies along the crystallographic c axis. The Cs^+ ions lie between the chains.

The absorption spectra of $CsMg_{1-x}V_xCl_3$ ($x = 0.01$–0.15) have been reported [29]. The temperature dependence of the bands in the region of $^2E\,^4A_2$ single excitations permitted the calculation of $2J = -187 \pm 5$ cm^{-1}. High energy bands were assigned to double excitations involving the ^2E and $^2T_1$ states. The polarizations in all cases matched those expected from a Tanabe mechanism.

Mn^{2+} has also been studied in $CsMgX_3$ (X = Cl, Br) [2]. In addition to the results discussed in Section B (i), several other temperature-sensitive sets of bands were noted in the spectra of both systems. These bands appear on the lower energy side of the $^4A_1\,^4E(G)$, $^4T_2(D)$, and $^4E(D)$ single-ion excitations and were attributed to pair excitations. For the chloride and bromide $2J$ was determined to be -39.2 cm^{-1} and -28.4 cm^{-1} respectively [2]. An important conclusion can be drawn from the following: for pure $CsMnBr_3$, $2J$ was determined to be -28.4 cm^{-1} from inelastic neutron scattering [116], and -27.6 cm^{-1} from magnetic susceptibility measurements [117], while in $CsMg_{0.80}Mn_{0.20}Br_3$ a value of -28.4 cm^{-1} was calculated for Mn^{2+} pairs from optical spectroscopy [2]. The conclusion is that in the one-dimensional antiferromagnet, $CsMnBr_3$, the nearest-neighbor interactions are dominant, and the next-nearest-neighbor interactions can to a good approximation be ignored in determining the strength of exchange coupling. This is in good agreement with inelastic neutron scattering studies of Mn^{2+} trimers in the mixed crystals, which revealed that the ratio of next-nearest to nearest-neighbor exchange was approximately 1/10 [118].

An intensive study of the spectra of $AFeX_3$ (A = Rb, Cs; X = Cl, Br) and $CsMg_{1-x}Fe_xCl_3$ ($x = 0.05$ and 0.12) has been reported [119]. A special feature of the spectra of the pure compounds was the greatly enhanced intensity (3–4 orders of magnitude) of the spin-forbidden bands over those found in isolated Fe^{2+} complexes. In the mixed crystal the intensities were

enhanced, but to a considerably smaller degree. The enhancements were attributed to exchange coupling between the Fe^{2+} ions.

Evidence for Co^{2+} ion-pair formation in $CsM_{1-x}Co_xBr_3$ (M = Mg, Cd; $x \leq 0.4$) was noted by Tomblin et al. [120] in the polarized Raman spectra. The Co^{2+} electronic Raman spectra at 15 K showed lines between 16 and 1374 cm^{-1} which could be attributed to Co^{2+} pairs. The spectra were fitted using various models, with the resulting $2J$ values ranging from -2.4 to -33.0 cm^{-1}. The researchers also discuss earlier work on this system.

McPherson and Stucky [121] have found evidence of Ni^{2+}–Ni^{2+} exchange interactions in the strong concentration dependence of the intensity of the spin-forbidden bands in the optical spectra of $CsMgCl_3$ and $CsMgBr_3$ doped with 5% Ni^{2+} ($T = 77$ K). The report also deals with the pure compounds $CsNiX_3$ (X = Cl, Br). Ackerman et al. [122] have also studied the optical spectra of $CsMgCl_3:Ni^{2+}$ at 5 K, as well as those of $RNiCl_3$ (R = Cs, Rb, $(CH_3)_4N$) and $CsNiBr_3$. They found evidence of exchange interactions and double excitations in several of the spectra. Neither report gives values for the exchange parameters. The single-crystal luminescence and absorption spectra and the luminescence decay times of $CsMg_{1-z}Ni_zX_3$ (X = Cl, Br; $z < 0.02$) have recently been reported [123].

McPherson and coworkers [124,125] noted that when trivalent ions such as Cr^{3+} and Mo^{3+} are introduced into diamagnetic $CsMX_3$ lattices, the trivalent ions tend to cluster in pairs with an M^{2+} vacancy in the center of the pair. This occurs even when the doping levels are less than one part per thousand, and appears to be due to rather strict charge-compensation requirements of the linear chain lattice. They found from ESR spectroscopy that the exchange interactions appear to be antiferromagnetic for Cr^{3+} pairs in $CsMgCl_3$ ($2J = -0.96$ cm^{-1}) and $CsMgBr_3$ ($2J = -1.42$ cm^{-1}) (data at 77 K). For Mo^{3+} pairs in the same lattices at 77 K, $2J = -2.75$ cm^{-1} and $2J = -5.6$ cm^{-1} respectively.

In addition to the quasi-one-dimensional lattices, AMX_3, the two-dimensional diamagnetic lattices, MX_2 (M = Cd, Mg; X = Cl, Br), have been used as matrices. $MgBr_2$ belongs to space group $P\bar{3}m1$ (D_{3d}^3), while the others belong to $R\bar{3}m$ (D_{3d}^5) [126]. All of them contain sheets of edge-sharing octahedra which are slightly trigonally distorted. In $Cd_{0.85}Mn_{0.15}Cl_2$, evidence for Mn dimers was noted by Trutia et al. [127]. A detailed study [28] of $Cd_{0.92}Mn_{0.08}Cl_2$ and $Cd_{0.85}Mn_{0.15}Br_2$ showed the existence of temperature-sensitive bands associated with the $^4A_1(G)$, $^4E(G)$, $^4T_2(D)$, and $^4E(D)$ states. The temperature variation of the bands was attributed to Mn^{2+} pairs and permitted the evaluation of $2J$ as -2.86 cm^{-1} and -2.66 cm^{-1} for the chloride and bromide respectively.

$CdCl_2$ has also served as a matrix for research on Fe^{2+}–Fe^{2+} exchange coupling. Wild and Day [128] studied three $CdCl_2$ crystals containing

different concentrations of Fe^{2+}. Some bands in the 20000–24000 cm^{-1} region were found to be temperature sensitive. This fact, together with the polarization and concentration dependence of the bands, led the researchers to ascribe them to ferromagnetically coupled in-plane pairs of Fe^{2+} ions. An analysis of a particularly well-resolved transition between 23440 and 23500 cm^{-1} revealed a ground state splitting of 3.5 cm^{-1}. The excited state was assigned to $^3T_2(^3G)$.

Wiltshire has studied $MgCl_2$ doped with Fe^{2+}, Co^{2+} and a mixture of these two ions [129]. From the temperature variation of the hot bands $\sim$ 19000 cm^{-1} (Co) and $\sim$ 23600 cm^{-1} (Fe) he calculated the separation of the lowest ground state levels for cobalt pairs (6.0 cm^{-1}) and iron pairs ($\sim$ 7.5 cm^{-1}), and found that they agree well with the separations calculated using exchange parameters proper to pure $CoCl_2$ and $FeCl_2$. In the crystals containing both Co^{2+} and Fe^{2+} a new hot band was observed. Its variation with temperature enabled a calculation of the separation of the lowest levels to be 3.6 cm^{-1}.

Trutia and Voda [130] have also studied the effects of exchange interaction on the spectra of Co^{2+} ions in $CdCl_2$. A detailed optical and magnetic study of the singly excited $^2T_1(^2H)$ pair spectra of Co^{2+} ions in $CdBr_2$ has been reported [131]. Magnetic fields up to 13 T were used and the trigonal field of the matrix was taken into account in fitting the spectra.

(ii) $A_3M_2X_9$ compounds

There exists a series of compounds of the type $A_3M_2X_9$ where A = Cs, Rb, M = Ti, V, Cr, Mo, W, and X = Cl, Br, I. Of these the chromium compounds have been most extensively studied as regards their exchange properties. $Cs_3Cr_2Cl_9$ has been shown to belong to space group $P6_3/mmc$ [132]. The structure of the vanadium analog has been confirmed to be the same [133], and the rest are assumed to have the same structure. There are two dimers per unit cell, each dimer containing three bridging and six terminal halogens, and the overall dimer symmetry is D_{3h}. All the dimers are lined up with their threefold axes parallel to the crystal c axis. This makes these compounds attractive for polarized single-crystal and MCD spectroscopy.

The compounds, $Cs_3Ti_2X_9$, have a particular attraction, since each Ti^{3+} ion has a single d electron and an orbitally degenerate $^2T_2$ ground state (octahedral notation). Accordingly, these complexes are model systems of exchange-coupled dimers for which the Heisenberg operator should not be applicable. They have stimulated a great deal of theoretical work [5,134–136], and a number of experimental techniques have been used to study them: magnetic susceptibility including single-crystal anisotropy [137], visible and

NIR absorption spectroscopy including MCD [137], IR absorption [137] and reflectivity [138], and inelastic neutron scattering (INS) [138]. From the magnetic susceptibility measurements it was determined that both chloride and bromide have essentially non-magnetic ground levels with the first magnetic level a few hundred cm^{-1} to higher energy. Briat et al. [137] studied $Cs_3Ti_2Cl_9$ and postulated a large trigonal splitting of 1500 cm^{-1} with the non-degenerate orbital component lower in energy. As a consequence they could use a Heisenberg formalism to treat the exchange, and they derived a value of $2J \approx -525$ cm^{-1}.

Leuenberger et al. [138] on the basis of their INS, IR reflectivity and magnetic susceptibility measurements on $Cs_3Ti_2Br_9$ reached a different conclusion. They derived a trigonal crystal-field parameter of the same order of magnitude as the exchange interaction and the spin–orbit coupling. As a consequence, a Heisenberg Hamiltonian was considered to be inadequate and the orbital degeneracy was explicitly taken into account. The exchange parameter V_0, which is related to $-J$ in a very general sense, was found to be 180 cm^{-1}.

Both $Cs_3V_2Cl_9$ and $Rb_3V_2Br_9$ have been studied experimentally (magnetic susceptibility, INS, optical absorption and MCD spectroscopy) [133]. As was the case for Ti^{3+}, the V^{3+} ion has an orbitally degenerate T ground state in an octahedral crystal field, and a Heisenberg Hamiltonian might be expected to be inadequate for the treatment of the exchange in $V_2X_9^{3-}$. In contrast to $Ti_2X_9^{3-}$, however, the exchange in $V_2X_9^{3-}$ is small compared with the intraionic crystal field. This places the trigonal $^3A_2$ component at lower energy, and as a consequence, a Heisenberg Hamiltonian may be appropriate. The principal result of the above-mentioned study is that in both compounds exchange and second-order spin–orbit coupling in the $^3A_2$ state are of the same order of magnitude (a few reciprocal centimeters). The exchange parameters were found to be ferromagnetic: for $Cs_3V_2Cl_9$ and $Cs_3V_2Br_9$ $2J = 11$ cm^{-1} and $2J = 5.2$ cm^{-1} respectively.

For $Cs_3Cr_2X_9$ the INS experiments have shown the following. (a) There is weak interdimer coupling (J') in addition to much stronger intradimer coupling. For example, in $Cs_3Cr_2Cl_9$ the ratio J'/J is approximately 1/50 [139]. (b) In the series $Cs_3Cr_2X_9$ (X = Cl, Br, I) the intradimer exchange decreases ($2J = -14.0$, -8.3 and -6.4 cm^{-1} respectively), while the interdimer exchange increases (Cl < Br < I).

Optical spectra have been recorded for these compounds. In particular, a great deal of work has appeared on the $^4A_2 \rightarrow {}^2T_1$ and $^4A_2 \rightarrow {}^2E$ single excitations. It should be noted that, in contrast with most Cr^{3+} complexes with O and N coordination, the weak ligand field supplied by the halogens causes the lowest excited state to be $^4T_2$ and not ^2E. The result is that sharp-line luminescence spectroscopy, which is usually very powerful for the

determination of exchange splittings in the ground state, cannot be used here. In all cases, however, low temperature polarized crystal absorption spectroscopy has been employed, accompanied by magnetic fields as external perturbations (Zeeman absorption and MCD spectroscopy).

Three groups have studied the same (or related) compounds with the same (or very similar) experimental techniques, but have used quite different theoretical models to interpret their results. This has made the results difficult to compare.

A group in Canberra has carried out detailed absorption, MCD and Zeeman spectroscopy on $Cs_3Cr_2Br_9$ [25]. The spectra exhibit sharper lines in the $^2E\,^4A_2$ and $^2T_1\,^4A_2$ region of the spectrum than are found in the chloro analog. The researchers found that both single-ion and exchange-induced intensity contribute to the single excitations of the chromium pair. Using the model developed by Dubicki and Tanabe [23], they achieved only moderate agreement between observed and predicted splitting patterns. Inclusion of spin–orbit coupling was found necessary for the interpretation of the MCD results. There is substantial disagreement, however, with other workers (see below) about the magnitude of the spin–orbit parameter. They also found non-vanishing intensity in the $\Delta S = 2$ pair transitions. This is somewhat unusual, but has been observed in some other chromium compounds such as chromium diol dimers [20,68,70]. They consider that this could be explained by the insertion of anisotropic exchange terms in the Hamiltonian. It may be said that this group of researchers chose a system with the sharpest lines, carried out all experiments with care, and used a theoretical model which had already proved useful in the study of Mn^{2+} pairs.

A group in Paris has carried out an extensive investigation of $Cs_3Cr_2Cl_9$ with polarized absorption and MCD spectroscopy down to 1.7 K [71]. The principal conclusion of interest is that most of the intensity in the ^2E, $^2T_1$ single-excitation region is due to a single-ion electric dipole mechanism, several transitions being vibrationally induced. The researchers found, however, a substantially larger spin–orbit parameter than the Canberra group found for the bromide. This is, of course, opposite to the normal trend for spin–orbit coupling constants. The exchange parameters which they calculate were, however, of the same order of magnitude as found for the bromide. This group of researchers also made measurements in the region of $^2E\,^2E$, $^2E\,^2T_1$ and $^2T_1\,^2T_1$ double excitations, but made no detailed analysis. While these experiments were elegant and carefully carried out, it can be noted that the lines in the spectra of the chloride overlap the $^4T_2$ band more strongly than in the case of the bromide, and this has limited the information content of the reported spectra.

In addition to these groups, a third group in Nottingham has done extensive work on $Rb_3Cr_2Cl_9$ [140], $Rb_3Cr_2Br_9$ [24], as well as on the

analogous Cs salts [141,142]. This group too used low temperature optical and Zeeman spectroscopy with large magnetic fields (up to 13 T). The theoretical model used is that proposed by Barry et al. [143] based on ideas suggested by Stevens [144]. As did the other groups, this group obtained from its spectra exchange parameters for the ground state and for the $^2E^4A_2$ and $^2T_1{}^4A_2$ excited states. In general, the results can be correlated reasonably well with those of Dubicki et al. [25]. An unusual conclusion from the Zeeman experiments, however, is that in both $Cs_3Cr_2Br_9$, and the Rb analog the g values are substantially reduced. The researchers find $g \sim 1.5$ for the ground state of both bromides, whereas for both chlorides the g values are normal. They explain the low values as being due to delocalization of electrons between bromide and chromium ions. This conclusion is open to some question, since for Cr^{3+} in Cs_2NaYBr_6, where the chromophore is also $CrBr_6{}^{3-}$, g has a normal value of 2.0 [145]. Furthermore, in the absorption spectrum of this chromophore there are not unusually low lying $Br^- \rightarrow Cr^{3+}$ CT transitions. Finally, the observation is at variance with the results of Dubicki et al. [25], who did not find unusually low g values for $Cs_3Cr_2Br_9$.

We may conclude that, although a substantial body of work has been carried out on these systems, many questions remain about the exact nature of their ground and excited states.

A spectroscopic study [146] of the mixed halide, $Cs_3Cr_2Cl_6Br_3$, has shown that the three bromines are terminal, but not statistically arranged. All three reside at one end of the chromophore leaving it with trigonal symmetry.

A study of $Cs_3Mo_2Cl_9$ [26] has shown that the principal features of the spectra can be explained on the basis of an exchange-coupled pair with relatively strong σ Mo–Mo interaction. The researchers note that the metal–metal bonding in this and the analogous tungsten compound can best be considered as one strong σ and two weak π bonds.

Although exchange striction is a well-known effect in magnetically ordered systems, its direct observation in experiment has not often been made. A particularly clear example is found in the Raman spectrum of $Cs_3Cr_2Cl_9$ [147]. The a_1 modes in the $Cr_2Cl_9{}^{3-}$ dimer are found to be very temperature sensitive and sidebands appear a few wavenumbers to higher energy as the temperature is raised. Thus, for example, the a_1 terminal stretch shows four components at 370, 372.5, 375.5 and 378 cm^{-1}, whose intensities follow the calculated populations of the spin levels of the $^4A_2{}^4A_2$ ground state. Thus the dimer levels with $S = 0$, 1, 2, 3 all have slightly different vibrational energies, i.e. they have slightly different force constants and equilibrium geometries. The striction effect is known to be large when the exchange depends strongly on the coordinates and when the coordinates correspond to bonds which are easily deformed. Both these criteria apply here. Thus the experimentally observed variation in vibrational energy is attributed to electron–phonon coupling.

The conspicuous trend of exchange parameters within the series $Ti_2Cl_9^{3-}$ ($-2V_0$, corresponding roughly to $2J \approx -360$ cm^{-1}) [5,22], $V_2Cl_9^{3-}$ ($2J \approx 11$ cm^{-1}) [133] and $Cr_2Cl_9^{3-}$ ($2J \approx -14$ cm^{-1}) [139] was rationalized by Extended Hückel MO calculations [22]. The antiferromagnetic contributions to the exchange parameters can be related to one-electron transfer integrals, which are proportional to energy differences between the plus and minus combinations of magnetic atomic orbitals. This procedure, which goes back to the definition of kinetic exchange [148], was also used by Hay et al. [32] to estimate exchange parameters. The result of this calculation for the above series was in surprisingly good agreement with the observed trend. We may then conclude that the Extended Hückel MO technique is able to reproduce a trend within a series of structurally related compounds, despite the fact that, because of the inherent approximations, it is rather unreliable for the calculation of absolute exchange-parameter values.

(iii) Polynuclear chromium(III) complexes

There exists a very extensive and intensive literature on this topic. Many examples have been used to illustrate the topics discussed earlier. Here we will discuss in more detail the principal complexes that have been studied.

The basic rhodo cation, $[(NH_3)_5CrOCr(NH_3)_5]^{4+}$, is the Cr^{3+} dimer with the strongest exchange coupling yet observed [33]. The Cr–O–Cr unit is linear with a very short Cr–O distance (1.80 Å). This makes a very efficient pathway for $Cr^{3+} \rightarrow Cr^{3+}$ and $O^{2-} \rightarrow Cr^{3+}$ electron transfer with consequent antiferromagnetic exchange. With z being the Cr–Cr axis, there is strong π overlap of xz and yz magnetic orbitals with the oxygen p_x and p_y orbitals respectively. There is an intense charge-transfer band, completely z polarized, centered at 36000 cm^{-1}. The nature of this band is not completely clear, but besides some oxygen → chromium electron-transfer character, it may also have some chromium → chromium ET character. In any case, it appears to be the principal source of intensity for the strong z polarized double excitation bands in the blue part of the spectrum (see Fig. 9).

The luminescence spectrum reported for basic rhodo chloride [149] is clearly due to acid rhodo impurities. No genuine emission has so far been found for the basic rhodo complex. The tetragonal ligand-field potential experienced by Cr^{3+} is considerably stronger than in any other known Cr^{3+} complex. The lowest excited state is therefore expected to be the tetragonal ^2E component of $^2T_1$ and to lie at such a low energy that emission is either quenched non-radiatively or is undetectable.

Two classical mono-hydroxo bridged complexes have been studied in great detail: acid rhodo, $[(NH_3)_5CrOHCr(NH_3)_5]^{5+}$, and acid erythro, $[(NH_3)_5CrOHCr(NH_3)_4(H_2O)]^{5+}$. The paper of Dubicki [19] on the latter

complex was the first study of a molecular Cr^{3+} dimer with a convincing theoretical interpretation; he used the Tanabe formalism. Since the Cr–O–Cr angle is between 160° and 170°, the complex could be approximated by a 180° model. The dominant antiferromagnetic orbital-exchange parameters are the same as in basic rhodo, $J_{xz\,xz}$ and $J_{yz\,yz}$.

A similar analysis has been made for acid rhodo [6,150–152]. In the spectrum of this complex the lowest levels of the first excited state are clearly due to $^2E^4A_2$ single excitations. Both the energy splittings and the intensity ratios conform to the Tanabe theory. At higher energies, however, there appears to be appreciable overlap between ^2E and $^2T_1$ single excitations, and unambiguous assignment of all the observed bands is no longer possible.

In both acid erythro and acid rhodo, J for the excited state was found to be larger than the ground state J by 30%–50%, in good agreement with theoretical expectations. Both complexes exhibit rich spectra in the region of ^2E and $^2T_1$ double excitations, but no detailed analysis has so far been made.

Besides the monohydrate there exists a trihydrate or dihydrate of $\{rhodo\}Cl_5$. Single-crystal luminescence [153] and absorption [150] spectra show that the electronic splittings of the latter complex are essentially the same as in the monohydrate. $2J = -31.9\ cm^{-1}$ and $j = 0.23\ cm^{-1}$ are the ground state parameters derived from the low temperature luminescence peaks.

Of the di-μ-hydroxo bridged complexes, the most studied are $[(en)_2Cr(OH)_2Cr(en)_2]X_4 \cdot 2H_2O$ and $[(NH_3)_4Cr(OH)_2Cr(NH_3)_4]Br_4 \cdot 4H_2O$ (X = Cl, Br) [20,21,154]. They were discussed briefly above in Section B (iii). The spectra of the NH_3–Cl compound in the region of $^2E^4A_2$ single excitations are extremely sharp, the bands having widths of less than $1\ cm^{-1}$ at 1.5 K. They are very rich and informative spectra. The sharp lines in both sets of compounds were studied by Zeeman spectroscopy, and the results were used to make unambiguous assignments of the absorption bands to the pair states and to determine orbital parameters and thus the principal exchange pathways.

The absorption spectrum of the NH_3–Cl complex was dramatically changed when a magnetic field was applied. Especially in the region of double excitations most of the sharp absorption bands disappeared when a magnetic field was applied at 2 K. This behavior, which seems very strange at first sight, can be explained as follows: since the ground-state exchange parameter is very small ($2J = -0.6\ cm^{-1}$), Zeeman energies are of the same order of magnitude as exchange-splitting energies for fields up to 5 T. As a result, spin crossovers will take place in the ground state multiplets as a function of applied magnetic field. At zero field the ground level is $|S = 0,$

$M_S = 0\rangle$, and with increasing fields the $|S = 1,\ M_S = -1\rangle$, $|S = 2,\ M_S = -2\rangle$ and $|S = 3,\ M_S = -3\rangle$ will successively become the ground level. Since all the doubly excited states have $S = 0$ and 1, and since the transitions are governed by the Tanabe selection rules, $\Delta S = 0$ and $\Delta M_S = 0$, it is evident that at low enough temperature all the double excitations will gradually disappear with increasing field. The low temperature absorption and luminescence spectra (in KBr pellets) of $[(NH_3)_4Cr(OH)_2Cr(NH_3)_4]Br_4 \cdot 4H_2O$ have also been reported [155].

Luminescence line narrowing in the diol complex, $[LCr(OH)_2(SO_4)CrL]S_2O_6 \cdot 3H_2O$ (L = bispicam = *N,N'*-bis(2-pyridylmethyl)amine) [68] has been treated in some detail in Section C (iii).

Tri-μ-hydroxo bridged Cr^{3+} dimers, $[LCr(OH)_3CrL]X_3$, have only recently been synthesized by Wieghardt et al. [156]. They can be made with very few ligands. Complexes with L = 1,4,7-trimethyl-1,4,7-triazacyclononane, X = ClO_4 (I) and Br (II), and L = 1,5,9-triazacyclononane, X = Br (III) have been synthesized and structurally and magnetically characterized (see refs. 4 and 66 and references cited therein). They are attractive systems for spectroscopic study, since they are very inert complexes, they possess relatively strong coupling and they have high trigonal symmetry. This latter property makes them analogous to the first nearest-neighbor pairs in ruby. The absorption spectra of (I) are shown in Fig. 5. The principal results of the research on this compound are as follows [4,157]. The spectra show extremely sharp absorption and luminescence bands (see Fig. 13). The Zeeman (Fig. 18) and MCD spectra provide the means of determining very accurate g values for the ground and excited states. As shown in Fig. 19, the first excited pair states are found to have extremely large $g \parallel c$ values, much higher than expected for an $^2E^4A_2$ excited state, more typical of $^2T_1{}^4A_2$ excited states. As a result of the trigonal ligand field and strong exchange, there is considerable mixing between excited states derived from $^2E(^2E)^4A_2$ and $^2E(^2T_1)^4A_2$. This was discussed in Section C (v). The luminescence spectra of the triol (III) have been reported in ref. 66 and were discussed in Section C (iii).

A comparison of the $^2E^4A_2$ splitting pattern in the various hydroxo-bridged complexes shows that in the monols and diols the lowest excited-state level has $S^* = 2$, while in the triols it has $S^* = 1$. This strange result for the monols and diols is due to the fact that so-called excitation-transfer integrals or resonance integrals of the form $\langle {}^2E^4A_2 \mid \hat{H}_{ex} \mid {}^4A_2{}^2E\rangle$ are non-zero. These off-diagonal matrix elements can be larger than the diagonal ones and thus lead to a splitting which looks ferromagnetic at first sight, although the underlying interactions are antiferromagnetic.

Low temperature (6–7 K) absorption and luminescence spectra have been reported for the hexahydroxo-bridged chromium cluster, $[Cr_4(OH)_6$-

$(NH_3)_{12}]Cl_6 \cdot 4H_2O$ and the deuterated analog [158]. Both ground and excited state splittings were seen in the optical spectra.

A large number of transition-metal compounds exist which contain the triangular cluster unit $[M_3O(RCOO)_6]^+$. Basic chromium(III) acetate, $[Cr_3O(CH_3COO)_6(H_2O)_3]Cl \cdot 6H_2O$ (CRAC) has been particularly extensively investigated (see refs. 159–163 and references cited therein). In their early absorption study, Dubicki and Day [159] observed complex bands in the 690–750 nm region due to exchange coupling between the three Cr^{3+} ions, as well as a high energy band system (330–365 nm) which was assigned to double excitations. About the same time, Ferguson and Güdel [161] showed by luminescence and excitation spectroscopy that at low temperature the crystals of CRAC contain two sets of inequivalent clusters. Exchange splittings and exchange parameters were very accurately determined for each of the two sets, and the parameters are correlated with deviations from the regular triangular structure of the complex at low temperatures. CRAC undergoes a phase transition at 211 K, and it was shown by X-ray diffraction [163] that there is a doubling of the unit cell at low temperature, which causes two inequivalent sets of molecules with different degrees of distortion to exist at low temperature. Two further sets of molecules are produced by dehydration, as was shown by site-selective spectroscopy [160]. The mechanism of energy transfer between the sets has also been extensively studied [160,162,163]. Intermolecular non-radiative energy transfer requires thermal activation. This is a result of the extreme "forbiddenness" of the transition between the lowest ground state level ($S = 1/2$) and the emitting level ($S = 7/2$) at low temperatures. Finally, it has been pointed out [164] that spectroscopic evidence rules out a dynamic distortion model [165] to explain the magnetic properties of this compound.

(iv) Dinuclear copper(II) complexes

There is currently a strong interest in Cu^{2+} dimer systems; for this several reasons can be adduced. The compounds show a very rich chemistry with a variety of structures and magnetic properties. Extensive magneto–structural correlations have been made [166], and these can be used in the design of new systems with very specific properties. Secondly, Cu^{2+} dimers are found in a number of active sites in proteins. A detailed study of their properties is necessary if their biological function is to be adequately understood. In this type of study optical spectroscopy has been used as one of many physical techniques mainly to obtain structural information about the active site. It is often coupled with MCD measurements, since the latter can distinguish between magnetic and nonmagnetic ground states. This area has been reviewed recently by Solomon et al. [167] (see also ref. 168).

One of the most studied Cu^{2+} dimer systems is copper acetate monohydrate, $(CuAc_2 \cdot H_2O)_2$. The structure has been determined by X-ray diffraction and the electronic properties have been elucidated by many experimental techniques such as magnetic susceptibility measurements, ESR, optical spectroscopy and inelastic neutron scattering. In addition, a number of theoretical models for the coupling have been developed. Work on these carboxylate systems has been summarized by Hendrickson [169].

In the solid state the simplest unit of the compound has the two Cu^{2+} ions symmetrically bridged by four acetate groups. The resulting symmetry is essentially D_{4h} with $C_4(z)$ lying along the H_2O–Cu–Cu–H_2O axis. The exchange coupling is antiferromagnetic with $2J = -298 \pm 4$ cm^{-1} [170]. Whether the coupling between the two Cu^{2+} ions depends on a superexchange interaction through the carboxylate bridges or rather on direct Cu^{2+}–Cu^{2+} bonding is still controversial. This is in contrast to the analogous Cr^{2+} and Mo^{2+} compounds in which the coupling is much stronger and metal–metal bonding is probably more important [171].

The optical absorption spectrum of $(CuAc_2 \cdot H_2O)_2$ has been studied by several groups (listed in ref. 172) and most recently a detailed and thorough investigation has been carried out by Dubicki [172], who recorded the polarized crystal spectra of the compound at various temperatures from room temperature to 4.2 K. The spectra show a band system (I) around 700 nm with slightly different maxima and intensities in the z and xy polarizations, the latter being more intense ($\epsilon \approx 300$ per monomer). In both polarizations the band maxima show a small shift to higher energy on cooling to 77 K, and the bands increase in size by 10%–15%. They can with little doubt be assigned to ligand-field transitions on the d^9 Cu^{2+}; they are single excitations. Like excitations in other exchange-coupled systems which are spin allowed in the single ion, they are essentially unaffected by the coupling.

Band II (360 nm, $\epsilon \approx 210$) is polarized along the Cu–Cu axis; it appears to be characteristic of dimeric Cu^{2+} complexes. This band lies at about two times the energy of the normal d–d band maximum. It was found to double in size as the crystal was cooled from 287 to 77 K and to increase only slightly on further cooling to 4.2 K. In the xy polarization there is a weak band at 325 nm ($\epsilon \approx 30$) which also increases in size on cooling; the exact amount could not be determined, since the band lies on the edge of very strong UV absorption. The temperature dependence indicates that both transitions originate from the singlet ($S = 0$) ground state level of the coupled dimer. Transitions from the triplet level are not seen, a rather unusual and highly relevant observation with respect to a possible assignment of the bands.

Hansen and Ballhausen [173], using a model of two weakly coupled

chromophores, assigned band II as a transition to a doubly-excited ligand-field state. A second possibility is that band II is a ligand → metal charge-transfer band. Dubicki [172] favors this assignment and on the basis of a CNDO/2 MO calculation assigns the near-UV bands as follows:

$(z\text{–}360\ \text{nm})\ {}^1A_{1g} \rightarrow {}^1A_{2u}\ \left[b_{2u}(p_y) \rightarrow b_{1g}(x^2\text{–}y^2)\right]$

$(xy\text{–}325\ \text{nm})\ {}^1A_{1g} \rightarrow {}^1E_u\ \left[e_g(p_x) \rightarrow b_{2u}(x^2\text{–}y^2)\right]$

He also states that the charge-transfer assignment can readily account for the observed intensity of the bands.

More light can be shed on this problem by a consideration of the spectra of $Cu_2Cl_6^{2-}$. Compounds containing this unit have a garnet red color. They were first investigated by Willett [174] and by Willett and Chow [175] and have most recently been the subject of an extensive investigation by Desjardins et al. [176], who studied a number of chlorocuprates, several of which contain the $Cu_2Cl_6^{2-}$ ion. The spectra all show the usual ligand-field single excitation bands in the 1000–670 nm (10000–15000 cm^{-1}) range. In addition, the crystals which contain the dimer, $Cu_2Cl_6^{2-}$, show a weak band around 20000 cm^{-1} ($\epsilon_{\text{per Cu}} \approx 40$–65). It is polarized along the Cu–Cu axis (x) in $LiCuCl_3 \cdot 2H_2O$ and $((CH_3)_2NH_2)CuCl_3$, but appears in both x and y polarizations in $KCuCl_3$ (xy determines the plane of the $Cu_2Cl_6^{2-}$ ion). The former two exhibit an effective C_{2h} symmetry in their spectra, while the latter, because of large variations in Cl_{ax}–Cu–Cl_{eq} angles, shows only C_i dimer symmetry. This band at 20000 cm^{-1} lies on the edge of a strong CT band ($\epsilon_{\text{per Cu}} \approx 3000$). The 20000 cm^{-1} band is very temperature sensitive; in $((CH_3)_2NH_2)CuCl_3$ and $KCuCl_3$ it increases in size on cooling, but decreases on cooling in $LiCuCl_3 \cdot 2H_2O$ (Fig. 21) [176]. As in copper acetate, this temperature dependence can be correlated with the magnetic properties, and it emerges that here also the intensity follows the singlet population. Thus in all three cases the band is assigned as a singlet excitation of the binuclear $Cu_2Cl_6^{2-}$ ion, with no corresponding triplet excitation observable.

The question of the exact nature of this dimer band, however, still remains unanswered. Does it involve a double excitation, or rather is it a charge-transfer (CT) transition? A careful analysis of the band shape, energy, and singlet intensity mechanism led Desjardins et al. [176] to reject the double excitation assignment. They argue that the alternate assignment as a singlet-to-singlet, non-bonding π ligand-to-copper CT excitation better fits the experimental data. This assignment, however, requires that the CT triplet-to-triplet absorption, which is not observed, must be several thousand wavenumbers to higher energy under the other, more readily assigned, CT bands. The researchers argue that in the $Cl^- \rightarrow Cu^{2+}$ CT states, which are shifted down in energy compared with those in the mononuclear $CuCl_4^{2-}$, the large singlet–triplet splitting is due to the magnetic orbitals having a

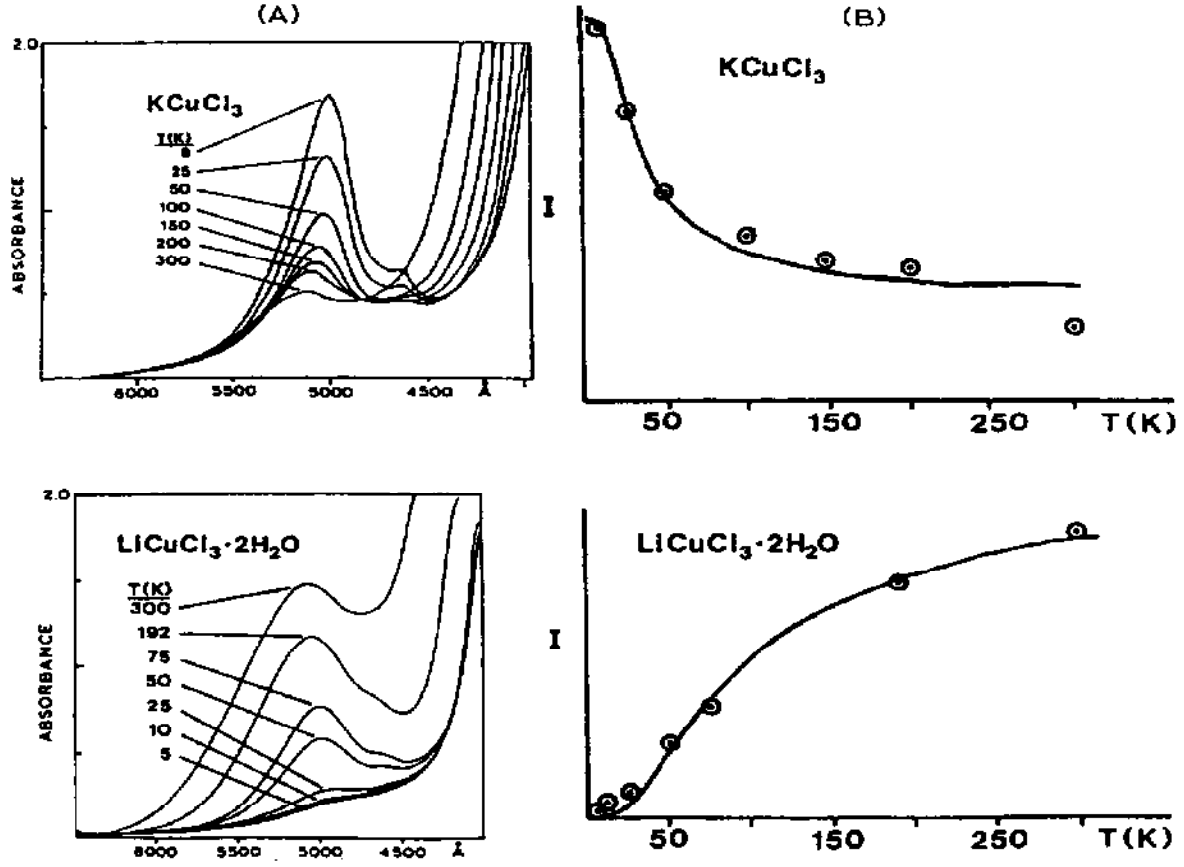

Fig. 21. (A) Temperature-dependent spectra of $Cu_2Cl_6^{2-}$ dimers. (B) Plots of integrated intensity (I) of the dimer bands vs. temperature. Solid lines correspond to the singlet ground state population [176]. (Reprinted with permission from Inorganic Chemistry. Copyright 1987 American Chemical Society.)

very favorable disposition for overlap. This leads to a large antiferromagnetic exchange interaction and a large splitting of the excited state. A value of 3555 cm^{-1} is reported from an Xα–SW study [177]. However, it must be noted that such calculations are unable to calculate double excitations and so automatically favor a CT explanation. Furthermore, this band has very low intensity for an allowed CT band; this clearly needs explanation. Finally, the doubly excited dimer states are known to lie in the same energy range. We would therefore expect substantial mixing between CT and double excitations, and a clear distinction may no longer be very meaningful.

(v) Iron(II) and iron(III) complexes

Fe^{2+} has some special features which make it suitable for the observation of pair spectra. It has only one spin-allowed transition around 9000–10 000

cm^{-1}. Above this transition lie a large number of spin-forbidden bands between about 15 000 and 30 000 cm^{-1}. Some are very sharp and show fine structure. In some compounds several of these spin-forbidden bands show strong temperature dependence. An example is provided by the mineral vivianite, $Fe_3(PO_4)_2 \cdot 8H_2O$, which contains phosphate-bridged Fe^{2+} pairs besides Fe^{2+} single ions. Its spectrum [63] shows the usual near-IR (NIR) $^5T_2 \rightarrow {}^5E$ band. This is split into two components separated by 3500 cm^{-1}, the splitting being attributed to a Jahn–Teller distortion of the excited state. A broad absorption around 15 200 cm^{-1}, which gives vivianite its light blue color, is due to an $Fe^{2+} \rightarrow Fe^{3+}$ intervalence electron transfer within Fe pairs on the surface, which have been partially oxidized by air. Between 18 000 and 28 000 cm^{-1} a number of weak sharp bands are seen. The spectrum of one of them at several temperatures is seen in Fig. 12. The band is strongly polarized, and its intensity goes to zero at very low temperature. This behavior is rather typical of exchange-coupled metal centers. The band is accordingly assigned to the pair of exchange-coupled Fe^{2+} ions. From the temperature dependence of the spectra the coupling constant in the ground state is calculated to be $2J = 5$ cm^{-1}.The lowest ground state level has $S = 4$, which indicates ferromagnetic coupling between the two Fe^{2+} ions. This was earlier determined by magnetic susceptibility and heat capacity measurements and confirmed by Mössbauer experiments (see ref. 63 for references to these measurements and to earlier room temperature optical spectra).

Dimeric, trimeric and tetrameric clusters of Fe^{2+} occur in the active sites of iron–sulfur proteins. A review of their low temperature absorption and MCD spectroscopic properties has recently appeared [178]. Typical of these centers, as well as of heme–iron proteins, is the presence of intense charge-transfer absorptions in the visible part of the spectrum. The absorption bands are not assigned, but used as "fingerprints" for identifying the various centers. In this sense, MCD provides an additional discriminating signature to the absorption spectra. None of the spectral features are typical of polymeric species in general.

The well-known complex, $[Fe_3O(CH_3COO)_6]^+$, has the same structure as the chromium analog, CRAC. Its deep red-brown color is due to a very intense absorption band in the UV which extends into and throughout the visible region. There are several shoulders and bands in this tail. One in particular ($\sim 22\,500$ cm^{-1} at 7 K) is considerably sharper than the others and could be due to the $^4A_1$ and ^4E single excitations. It appears to increase in intensity on cooling. An isolated broad band centered at 10 200 cm^{-1} ($\epsilon \approx 10$ per Fe) could be the first d–d band, $^6A_1 \rightarrow {}^4T_1$. It is at least 100 times as intense as the same transition in a mononuclear octahedral Fe^{3+} complex. The intensity enhancement is due to the exchange coupling and to the band's proximity to the CT absorption band [145].

There are many complexes known which contain the Fe^{3+}–O^{2-}–Fe^{3+} group, and a large number have been studied magnetically. The optical spectra of relatively few, however, have been reported. Of late there has been renewed interest because of the occurrence of a dinuclear Fe^{3+} center in hemerythrin and some enzymes. Solomon and Wilcox [168] give a summary of current understanding of the coupled binuclear iron site. An example of a study of model systems is provided by Schugar et al. [179], who reported the spectra of the oxo-bridged Fe^{3+} dimer, $Na_4[(FeEDTA)_2O] \cdot 12H_2O$ (EDTA = ethylenediaminetetraacetate), and some related compounds. $2J$ was found to be about -190 cm^{-1}. The principal spectral effects relating to exchange were the marked intensity enhancement of the one-center Fe^{3+} ligand-field bands, and the appearance of several bands between 240 and 350 nm with ϵ values of the order of 10^3. Because their energies correspond closely to the sums of the energies of individual Fe^{3+} ion transitions, they were assigned as double excitations of the Fe^{3+} pairs. The ϵ values suggest, however, that the bands have considerable CT character mixed in.

The spectra of polynuclear Fe^{3+} complexes containing both small and large iron aggregates were reviewed by Gray [180] several years ago.

(vi) Vanadyl dimers

An interesting pair of dimeric anions are $[(VO)_2(d\text{-tart})_2]^{4-}$ and $[(VO)_2(d\text{-tart})(l\text{-tart})]^{4-}$ (tart = tartrate ion). These d^1–d^1 bridged dimers have unusual magnetic properties. Magnetic susceptibility measurements give $2J = 140$ cm^{-1} for the NH_4^+ salt of the former [181] and $2J = 4.5$ cm^{-1} for the Na^+ salt of the latter [182]. The coupling is accordingly strongly ferromagnetic in the d,d complex. The difference in magnetic properties is reflected in the absorption spectra of the Na^+ salts [145]. The first absorption band in the d,l dimer is quite similar in position to that in $VO(acac)_2$ and $VOSO_4$, but shows greater splitting due to the low symmetry. The first absorption band of the d,d dimer, however, is lower in energy by several thousand cm^{-1}, with the first electronic origin at ~ 9300 cm^{-1}. This band also shows sharp fine structure, a feature found in no other vanadyl spectrum. The sharp bands form a progression in 850 cm^{-1}, the V–O stretching frequency, reduced from the ground state value of 950 cm^{-1}. This indicates a non-bonding → antibonding electronic transition. The spectra show no evidence of splittings due to exchange. The d,d complex is geometrically highly distorted, and this must be responsible for both the large ferromagnetic J value and the unusual spectra. A number of dinuclear Cu^{2+} complexes as well as a mixed Cu^{2+}/vanadyl^{2+} complex with strong ferromagnetic coupling ($2J > 100$ cm^{-1}) have been prepared and characterized by Kahn and coworkers in the past ten years (ref. 183, p. 57).

(vii) 4d and 5d dimers

Very little work on the optical spectroscopy of exchange coupled $4d$ and $5d$ complexes is found in the literature. Besides $Cs_3Mo_2Cl_9$ and the tungsten analog discussed in Section D (ii), the following studies are worth mentioning.

Bernstein and Meredith [184] observed pair spectra of Re(VI) when this was in the host lattices UF_6, MoF_6 and WF_6. This was but a small part of an extensive study of the electronic spectra of ReF_6. They conclude that the interactions are dominated by superexchange, and that the pathway is based on low lying delocalized charge-transfer bands.

Evidence of exchange coupling has been found in the NIR electronic absorption and MCD spectra of mulls of $[(NH_3)_5Os(L)Os(NH_3)_5]^{6+}$ (L = 4,4′-bipyridine and pyrazine) [185]. In the latter compound there was a striking temperature dependence of the bands. In the former the much weaker exchange coupling was determined by the presence of B terms in the MCD spectrum. Evidence for exchange coupling was not found in the spectrum of $[(NH_3)_5Os(pyrazine)Rh(NH_3)_5]^{6+}$.

(viii) Lanthanide(III) dimers

The sharp-line spectra of salts doped with lanthanide (Ln^{3+}) ions often contain satellite lines of lower intensity. In many cases they are due to lanthanide ions occupying inequivalent sites or to pair interactions. Prinz and Cohen [186] studied the satellites of several electronic transitions of Nd^{3+} doped in various lanthanide chlorides. They noted that the detailed structure of the satellites indicates near-neighbor interactions between Nd^{3+} and the lanthanide ions of the host. Leask and Smith shortly after this reported a study of the Gd^{3+}–Dy^{3+} pair interactions in $Gd_{0.98}Dy_{0.02}Cl_3$ [187]. Satellite lines have more recently been studied in detail by a number of groups using a variety of techniques, most involving sophisticated laser spectroscopy. Fricke [188] studied satellite lines in the absorption spectra of Pr^{3+}-doped $LaCl_3$ crystals. Pelletier-Allard and Pelletier [189] used excitation spectroscopy to study the $^4I_{9/2} \rightarrow {}^4G_{5/2}$ transition of Nd^{3+} in $Nd_xLa_{1-x}Cl_3$ ($x = 0.0005$) and $Nd_xPr_xLa_{1-2x}Cl_3$ ($x = 0.0005$). By this means they were able to assign different satellite lines to definite clusters of ions.

Pr^{3+}-doped LaF_3 has also been the subject of several studies by Buisson and coworkers [190–192]. They measured the energy transfer rates between two Pr^{3+} ions associated as a pair, and were able to identify about ten different classes of pairs. They did this by selective excitation of each class of pairs, making use of the fact that each class is associated with a given

satellite of the main line, which itself is due to isolated ions. They note that in general the farther the satellite is from the main line, the nearer to each other are the ions in the pair.

The same group has also studied Nd^{3+}-doped $LiYF_4$ and assigned the satellites to the various classes of pairs. They prove the existence of a short-range interaction which they interpret as superexchange [193,194]. Hunt and Pappalardo [195] have investigated the dye-laser excitation spectra of the technologically important $Y_2O_3:Eu^{3+}$ phosphors. Satellite structure in the excitation lines of the $^5D_0$ and $^5D_1$ manifolds were attributed to ion pairs. Wright and coworkers have studied the fluorescence spectra of pairs in PbF_2 doped with Eu^{3+} [196] and with Er^{3+} [197].

Dieke and coworkers, in two studies of $PrCl_3$, were the first to report spectroscopic evidence for double excitations in a lanthanide compound. In the excitation spectrum [198] they observed levels which corresponded very closely to the sum of two single excitations. Finer detail was observed later in a study of the absorption spectrum [199]. For example, the sum of $^3P_0 + {}^3F_2 = 25\,410.6$ cm^{-1} (the Stark component of each transition is zero) and there is a peak observed in the absorption spectrum at 25 410.8 cm^{-1}.

Dexter [200] was the first to provide a theoretical explanation for such double excitations which, since they are two-electron processes, are forbidden in a zero-order approximation. He employed first-order perturbation theory and showed that the prohibition could be overcome by considering the electronic interactions between the ions, neglecting, however, the overlap of the wavefunctions on the two ion centers. In this approach the intensity of the double excitation is stolen from allowed electronic transitions on the individual ions. We should note the formal analogy between this treatment and Dexter's theory of nonradiative excitation energy transfer in coupled systems [201]. Since the theory omits consideration of any overlap between the two centers, it is applicable to any system of weakly coupled chromophores.

Among the lanthanides, Yb^{3+} is particularly attractive because the only f–f transitions, $^2F_{7/2} \rightarrow {}^2F_{5/2}$, occur around 10 000 cm^{-1}. The spectrum is then transparent up to at least 30 000 cm^{-1}, where the first ligand-to-metal charge-transfer absorption is expected. It is found, for example, around 38 000 cm^{-1} in $YbCl_6^{3-}$ [202]. In particular, the region of possible double excitations around 20 000 cm^{-1} is clear. Schugar et al. [203] have observed double excitations in the electronic spectra of Yb_2O_3 and YbOF in this region.

Yen and coworkers [204,205] have studied possible double excitations in Yb^{3+} pairs in CaF_2 and in a silicate glass. In the $CaF_2:Yb^{3+}$ system, while monitoring the "normal" $^2F_{5/2} \rightarrow {}^2F_{7/2}$ luminescence around 10 000 cm^{-1}, the excitation spectrum showed a number of distinct features in the 20 000

cm^{-1} region which the researchers tentatively assigned as double excitations. The principal problem, which is typical of lanthanide systems, is that of identification. These double excitations are very weak, and since all the lanthanides, because of their similar chemistry, always occur as impurities in a given lanthanide, it is extremely difficult to exclude contributions from lanthanides other than Yb^{3+}.

Double excitations of Nd^{3+} pairs in LaF_3 by two-photon processes have also been reported by Buisson et al. [206].

There has existed for the past 20 years a strong interest in the mechanisms of excitation energy transfer in crystals and glasses doped with transition metal and lanthanide ions. A practical reason for this lies in the phenomenon of concentration quenching of the luminescence, which can be troublesome when searching for laser materials with high yields. In this concentration–quenching process, energy transfer between ions which are spatially close enough together plays an important part. This is essentially a pair effect, and the Förster/Dexter formalism for nonradiative energy transfer can be applied. In that formalism energy transfer takes place from a donor to an acceptor, i.e. within a pair of ions.

There exists an enormous body of literature—books, conference proceedings and reviews—on the subject of energy transfer. The interested reader will find extensive coverage in refs. 207–209.

REFERENCES

1 S.M. Jacobsen, H.U. Güdel and W.E. Smith, Inorg. Chem., 26 (1987) 2001.
2 P.J. McCarthy and H.U. Güdel, Inorg. Chem., 23 (1984) 880.
3 A.L. Schawlow, D.L. Wood and A.M. Clogston, Phys. Rev. Lett., 3 (1959) 271.
4 H. Riesen and H.U. Güdel, Mol. Phys., 60 (1987) 1221.
5 B. Leuenberger and H.U. Güdel, Mol. Phys., 51 (1984) 1; see refs. 7–14 therein.
6 H. Riesen and H.U. Güdel, Mol. Phys., 58 (1986) 509.
7 P. Day and L. Dubicki, J. Chem. Soc., Faraday Trans. 2, 69 (1973) 363.
8 J. Ferguson, H.J. Guggenheim and Y. Tanabe, J. Phys. Soc. Jpn., 21 (1966) 692.
9 K. Gondaira and Y. Tanabe, J. Phys. Soc. Jpn., 21 (1966) 1527.
10 Y. Tanabe, T. Morija and S. Sugano, Phys. Rev. Lett., 15 (1965) 1023.
11 G.L. McPherson, T.J. Kistenmacher and G.D. Stucky, J. Chem. Phys., 52 (1970) 815.
12 M. Naito, J. Phys. Soc. Jpn., 34 (1973) 1491.
13 L. Dubicki and J. Ferguson, Chem. Phys. Lett., 68 (1979) 507.
14 J.B. Goodenough, Magnetism and the Chemical Bond, Interscience, New York, 1976.
15 J. Kanamori, J. Phys. Chem. Solids, 10 (1959) 87.
16 J.P. van der Ziel, Phys. Rev. B, 4 (1971) 2888.
17 M. Gutowski, Phys. Rev. B, 18 (1978) 5984.
18 G.G.P. van Gorkom, J.C.M. Henning and R.P. van Stapele, Phys. Rev. B, 8 (1973) 955.
19 L. Dubicki, Aust. J. Chem., 25 (1972) 739.
20 S. Decurtins and H.U. Güdel, Inorg. Chem., 21 (1982) 3598.
21 S. Decurtins, H.U. Güdel and A. Pfeuti, Inorg. Chem., 21 (1982) 1101.

22 B. Leuenberger and H.U. Güdel, Inorg. Chem., 25 (1986) 181.
23 L. Dubicki and Y. Tanabe, Mol. Phys., 34 (1977) 1531.
24 N.J. Dean and K.J. Maxwell, Chem. Phys., 106 (1986) 233. See also references cited therein.
25 L. Dubicki, J. Ferguson and B.V. Harrowfield, Mol. Phys., 34 (1977) 1545.
26 L. Dubicki, E.R. Krausz, R. Stranger, P.W. Smith and Y. Tanabe, Inorg. Chem., 26 (1987) 2247.
27 J. Ferguson, H.U. Güdel, E.R. Krausz and H.J. Guggenheim, Mol. Phys., 28 (1974) 893.
28 P.J. McCarthy and H.U. Güdel, Inorg. Chem., 25 (1986) 838.
29 H. Riesen and H.U. Güdel, Inorg. Chem., 23 (1984) 1880.
30 J. Glerup, D.J. Hodgson and E. Pedersen, Acta Chem. Scand. Ser. A, 37 (1983) 161.
31 H.U. Güdel, ACS Symp. Ser., 307 (1986) 1.
32 P.J. Hay, J.C. Thibeault and R. Hoffmann, J. Am. Chem. Soc., 97 (1975) 4884.
33 H.U. Güdel and L. Dubicki, Chem. Phys., 6 (1974) 272.
34 H.U. Güdel, Chem. Phys. Lett., 36 (1975) 328.
35 T. Tsuboi and W. Kleeman, J. Magn. Magn. Mater., 31–34 (1983) 577.
36 J.P. van der Ziel, Phys. Rev. B, 9 (1974) 2846.
37 J.P. van der Ziel, J. Chem. Phys., 57 (1972) 2442.
38 S.S. Kim, S.A. Reed and J.W. Stout, Inorg. Chem., 9 (1970) 1584.
39 W.E. Smith, J. Chem. Soc. A, (1969) 2677.
40 A. Hauser and H.U. Güdel, Chem. Phys. Lett., 82 (1981) 72.
41 G.L. McPherson, T.J. Kistenmacher, J.B. Folkers and G.D. Stucky, J. Chem. Phys., 57 (1972) 3771.
42 J. Ferguson, T.E. Wood and H.J. Guggenheim, Inorg. Chem., 14 (1975) 177.
43 J. Ferguson, T.E. Wood and H.J. Guggenheim, Aust. J. Chem., 25 (1972) 453.
44 J. Ferguson and H.J. Guggenheim, J. Chem. Phys., 44 (1966) 1095.
45 J. Ferguson, Aust. J. Chem., 21 (1968) 323; Prog. Inorg. Chem., 12 (1970) 160.
46 M. Regis and Y. Farge, J. Phys., 37 (1976) 627.
47 D.R. Wilson, D.H. Brown and W.E. Smith, Inorg. Chem., 25 (1986) 898; Chem. Phys. Lett., 84 (1981) 552.
48 S.M. Jacobsen and H.U. Güdel, J. Lumin., 38 (1987) 184.
49 S.M. Jacobsen, W.E. Smith, C. Reber and H.U. Güdel, J. Chem. Phys., 84 (1986) 5205.
50 J.S. Helman and W. Baltensperger, Phys. Rev. B, 25 (1982) 6847.
51 T. Kita and Y. Tanabe, J. Phys. Soc. Jpn., 54 (1985) 2293.
52 T. Kita and Y. Tanabe, J. Phys. Soc. Jpn., 54 (1985) 2304.
53 J. Murphy and R.C. Ohlmann, in H.M. Crosswhite and H.W. Moos (Eds.), Optical Properties of Ions in Crystals, Interscience, New York, 1967, p. 239.
54 M. Matsuoka, M.A. Aegerter, H. Panepucci, M.C. Terrile, J.S. Helman and H.J. Scheel, Phys. Rev. Lett., 50 (1983) 204.
55 J.P. van der Ziel and L.G. van Uitert, Phys. Rev., 180 (1969) 343; Phys. Rev. Lett., 21 (1968) 1334.
56 J.P. van der Ziel and L.G. van Uitert, Phys. Rev. B, 8 (1973) 1889.
57 K. Aoyagi, M. Kajiura and S. Sugano, J. Phys. Soc. Jpn., 50 (1981) 3725.
58 H. Szymczak, W. Wardzynski and V.I. Sokolov, Physica B+C, 86–88 (1977) 1221.
59 J. Ferre and M. Regis, Solid State Commun., 26 (1978) 225.
60 H.J.W.M. Hoekstra, C.R. Ronda and C. Haas, Physica B+C, 122 (1983) 295.
61 T.E. Wood, P.A. Cox, P. Day and P.J. Walker, J. Phys. C, 15 (1982) L787.
62 J. Ferguson, H.J. Guggenheim and Y. Tanabe, J. Chem. Phys., 45 (1966) 1134.
63 H.U. Güdel, Inorg. Chem., 22 (1983) 3812.

64 B. DiBartolo (Ed.), Luminescence of Inorganic Solids, Plenum, New York, 1978.
65 J. Ferguson, H.J. Guggenheim and Y. Tanabe, J. Appl. Phys., 36 (1965) 1046.
66 H. Riesen, C. Reber, H.U. Güdel and K. Wieghardt, Inorg. Chem., 26 (1987) 2747.
67 W.M. Yen and R.T. Brundage, J. Lumin., 36 (1987) 209; see also the other articles in this issue, nos. 4 and 5.
68 H. Riesen and H.U. Güdel, Chem. Phys. Lett., 133 (1987) 429.
69 S. Larsen, K. Michelsen and E. Pedersen, Acta Chem. Scand. Ser. A, 40 (1986) 63.
70 C. Reber, H.U. Güdel, L. Spiccia and W. Marty, Inorg. Chem., 26 (1987) 3186.
71 B. Briat, M.F. Russel, J.C. Rivoal, J.P. Chapelle and O. Kahn, Mol. Phys., 34 (1977) 1357.
72 H. Riesen and H.U. Güdel, J. Chem.Phys., 87 (1987) 3166.
73 G.J. Piermarini, S. Block, J.D. Barnett and R.A. Forman, J. Appl. Phys., 46 (1975) 2774.
74 W. Platz and J. Heber, Z. Phys. B, 24 (1976) 333.
75 J. Ferguson and B. van Oosterhout, J. Lumin., 18–19 (1979) 165.
76 J. Ferguson and B. van Oosterhout, Solid State Commun., 27 (1978) 1223.
77 S.A. Basun, A.A. Kaplyanskii and S.P. Feofilov, Fiz. Tverd. Tela (Leningrad), 28 (1986) 3616; Chem. Abstr., 106 (1987) 185325h.
78 V.Ya. Mitrofanov, A.E. Nikiforov, V.A. Sapozhnikov and A.N. Men, Solid State Commun., 16 (1975) 899.
79 Q. Williams and R. Jeanloz, Phys. Rev. B, 31 (1985) 7449.
80 J. Heber and W. Platz, J. Lumin., 18–19 (1979) 170.
81 A. Monteil and E. Duval, J. Lumin., 18–19 (1979) 793.
82 A. Wasiela, Y.M. D'Aubigne and D. Block, J. Lumin., 36 (1986) 11.
83 A. Wasiela, D. Block and Y.M. D'Aubigne, J. Lumin., 36 (1986) 23.
84 G.F. Imbusch, in B. DiBartolo (Ed.), Energy Transfer Processes in Condensed Matter, Plenum, New York, 1984, p. 471.
85 F.I. Hasan, P.J. King, D.T. Murphy and V.W. Rampton, J. Phys. C, 12 (1979) L513.
86 J. Ferguson and P.E. Fielding, Aust. J. Chem., 25 (1972) 1371.
87 J.P. van der Ziel, Phys. Rev. Lett., 26 (1971) 766.
88 H. Siebold and J. Heber, J. Lumin., 23 (1981) 325.
89 V.Ya. Mitrofanov, V.A. Sapozhnikov, A.E. Nikiforov and A.N. Men, J. Magn. Magn. Mater., 20 (1980) 141.
90 M. Sasaki, NHK (Nippon Hoso Kyokai) Gijutsu Kenkyu, 26 (1974) 94; Chem. Abstr., 82 (1975) 66232b.
91 G.G.P. van Gorkom, Phys. Rev. B, 8 (1973) 1827.
92 D.L. Wood, G.F. Imbusch, R.M. Macfarlane, P. Kisliuk and D.M. Martin, J. Chem. Phys., 48 (1968) 5255.
93 J. Derkosch, W. Mikenda and A. Preisinger, J. Solid State Chem., 22 (1977) 127.
94 H. van den Boom, J.J. van Dijsseldonk and J.C.M. Henning, J. Chem. Phys., 66 (1977) 2368.
95 R.C. Powell, Liu Xi, Xu Gang, G.J. Quarles and J.C. Walling, Phys. Rev. B, 32 (1985) 2788. See also R.C. Powell, J. Phys., Colloq., C7 (1985) 403.
96 B.D. MacCraith, T.J. Glynn, G.F. Imbusch, J.P. Rameika and D.L. Wood, Phys. Rev. B, 25 (1982) 3572; J. Lumin., 24–25 (1981) 269.
97 C.M. McDonagh and B. Henderson, J. Phys. C, 18 (1985) 6419; J. Lumin., 31–32 (1984) 269.
98 A. Boyrivent, M. Ferrari, E. Duval and A. Monteil, J. Phys. C, 19 (1986) 3253.
99 G. Grinvalds and N.A. Mironova, Phys. Stat. Solidi B, 99 (1980) K101.
100 I.V. Skorobogatova and A.I. Zvyagin, Opt. Spektrosk., 33 (1972) 594; Chem. Abstr., 78 (1973) 22037e.

101 A.I. Bakhtin and V.M. Vinokurov, Geokhimiya, 1 (1978) 87; Chem. Abstr., 88 (1978) 139407y.
102 G. Smith, Phys. Chem. Miner., 3 (1978) 375.
103 P.J. McCarthy and H.U. Güdel, unpublished results, (1984).
104 N.S. Al'tshuler and M.V. Eremin, Fiz. Tverd. Tela (Leningrad), 21 (1979) 181; Chem. Abstr., 90 (1979) 129848v.
105 W.A. Sibley and N. Koumvakalis, Phys. Rev. B, 14 (1976) 35.
106 L. Dubicki, J. Ferguson and H. Masui, Mol. Phys., 39 (1980) 661.
107 J. Ferguson, H. Masui and Y. Tanabe, Mol. Phys., 37 (1979) 737.
108 J. Ferguson and H. Masui, J. Lumin., 18–19 (1979) 224.
109 J. Ferguson and H. Masui, J. Phys. Soc. Jpn., 42 (1977) 1640.
110 S.R.P. Smith and J. Owen, J. Phys. C, 4 (1971) 1399.
111 J. Ferguson, H.U. Güdel and E.R. Krausz, Mol. Phys., 30 (1975) 1139.
112 J. Ferguson, H.J. Guggenheim and Y. Tanabe, Phys. Rev., 161 (1967) 207.
113 J. Ferguson, J. Lumin., 18–19 (1979) 159.
114 J. Ferguson, H.J. Guggenheim and E.R. Krausz, J. Phys. C, 4 (1971) 1866.
115 U. Schmid, H.U. Güdel and R.D. Willett, Inorg. Chem., 21 (1982) 2977.
116 W. Breitling, W. Lehmann, R. Weber, N. Lehner and V. Wagner, J. Magn. Magn. Mater., 6 (1977) 113.
117 M. Eibschütz, R.C. Sherwood, F.S.L. Hsu and D.E. Cox, AIP Conf. Proc., 10 (1972) 684.
118 U. Falk, A. Furrer, N. Furer, H.U. Güdel and J.K. Kjems, Phys. Rev. B, 35 (1987) 4893.
119 C.F. Putnik, G.M. Cole, B.B. Garrett and S.L. Holt, Inorg. Chem., 15 (1976) 826.
120 C.W. Tomblin, G.D. Jones and R.W.G. Syme, J. Phys. C, 17 (1984) 4345.
121 G.L. McPherson and G.D. Stucky, J. Chem. Phys., 57 (1972) 3780.
122 J. Ackerman, E.M. Holt and S.L. Holt, J. Solid State Chem., 9 (1974) 279.
123 C. Reber and H.U. Güdel, Inorg. Chem., 25 (1986) 1196.
124 G.L. McPherson, W. Heung and J.J. Barraza, J. Am. Chem. Soc., 100 (1978) 469.
125 G.L .McPherson, J.A. Varga and M.H. Nodine, Inorg. Chem., 18 (1979) 2189.
126 R.W.G. Wycoff, Crystal Structures, 2nd Edn., Interscience, New York, 1965, Vol. 1, 268 ff.
127 A. Trutia, V. Ghiordanescu and M. Voda, Phys. Stat. Solidi B, 70 (1975) K19.
128 J.B. Wild and P. Day, J. Phys. C, 10 (1977) 4079.
129 M.C.K. Wiltshire, J. Phys. C, 15 (1982) 4177.
130 A. Trutia and M. Voda, Rev. Fiz. Chim., Ser. A, 7 (1970) 301; Chem. Abstr., 74 (1970) 36571d.
131 I.W. Johnstone, K.J. Maxwell and M.G. Read, J. Magn. Magn. Mater., 15–18 (1980) 819.
132 G.J. Wessel and D.J.W. Ijdo, Acta Crystallogr., 10 (1957) 466.
133 B. Leuenberger, B. Briat, J.C. Canit, A. Furrer, P. Fischer and H.U. Güdel, Inorg. Chem., 25 (1986) 2930.
134 M. Drillon and R. Georges, Phys. Rev. B, 24 (1981) 1278.
135 M. Drillon and R. Georges, Phys. Rev. B, 26 (1982) 3882.
136 O. Kahn, Mol. Phys., 31 (1976) 957.
137 B. Briat, O. Kahn, I. Morgenstern-Badarau and J.C. Rivoal, Inorg. Chem., 20 (1981) 4193.
138 B. Leuenberger, H.U. Güdel and A. Furrer, Chem. Phys. Lett., 126 (1986) 255.
139 B. Leuenberger, A. Stebler, H.U. Güdel, A. Furrer, R. Feile and J.K. Kjems, Phys. Rev. B, 30 (1984) 6300.
140 N.J. Dean and K.J. Maxwell, Mol. Phys., 47 (1982) 551.

141 N.J. Dean and K.J. Maxwell, J. Magn. Magn. Mater., 31–34 (1983) 563.
142 I.W. Johnstone, K.J. Maxwell and K.W.H. Stevens, J. Phys. C, 14 (1981) 1297.
143 K.R. Barry, K.J. Maxwell, K.A. Siddiqui and K.W.H. Stevens, J. Phys. C, 14 (1981) 1281.
144 K.W.H. Stevens, Phys. Rep., 24 (1976) 1.
145 H.U. Güdel, unpublished results, (1987).
146 S.E. Butler, P.W. Smith, R. Stranger and I.E. Gray, Inorg. Chem., 25 (1986) 4375.
147 I.W. Johnstone, B. Briat and D.J. Lockwood, Solid State Commun., 35 (1980) 689.
148 P.W. Anderson, Solid State Phys., 14 (1963) 99.
149 M. Morita and S. Shionoya, J. Phys. Soc. Jpn., 28 (1970) 134, 144.
150 P. Engel and H.U. Güdel, Inorg. Chem., 16 (1977) 1589.
151 J. Ferguson, H.U. Güdel and M. Puza, Aust. J. Chem., 26 (1973) 513.
152 H. Riesen and H.U. Güdel, Inorg. Chem., 25 (1986) 3566.
153 J. Ferguson and H.U. Güdel, Aust. J. Chem., 26 (1973) 505.
154 A. Beutler, H.U. Güdel, T.R. Snellgrove, G. Chapuis and K.J. Schenk, J. Chem. Soc., Dalton Trans., (1979) 983.
155 M. Morita, T. Schönherr, R. Linder and H.H. Schmidtke, Spectrochim. Acta, Part A, 38 (1982) 1221.
156 K. Wieghardt, P. Chaudhuri, B. Nuber and J. Weiss, Inorg. Chem., 21 (1982) 3086.
157 H. Riesen, H.U. Güdel, P. Chaudhuri and K. Wieghardt, Chem. Phys. Lett., 110 (1984) 552.
158 H.U. Güdel, U. Hauser and A. Furrer, Inorg. Chem., 18 (1979) 2730.
159 L. Dubicki and P. Day, Inorg. Chem., 11 (1972) 1868.
160 L. Dubicki, J. Ferguson and B. Williamson, Inorg. Chem., 22 (1983) 3220.
161 J. Ferguson and H.U. Güdel, Chem. Phys. Lett., 17 (1972) 547.
162 M. Morita and Y. Kato, J. Quantum Chem., 18 (1980) 625.
163 K.J. Schenk and H.U. Güdel, Inorg. Chem., 21 (1982) 2253.
164 H.U. Güdel, J. Chem.Phys., 82 (1985) 2510.
165 D.H. Jones, J.R. Sams and R.C. Thompson, J. Chem. Phys., 81 (1984) 440.
166 R.D. Willett, in R.D. Willett, D. Gatteschi and O. Kahn (Eds.), Magneto-structural Correlations in Exchange Coupled Systems, Reidel, Dordrecht, 1983, p. 389.
167 E.I. Solomon, K.W. Penfield and D.E. Wilcox, Struct. Bonding (Berlin), 53 (1983) 1.
168 E.I. Solomon and D.E. Wilcox, in R.D. Willett, D. Gatteschi and O. Kahn (Eds.), Magneto-structural Correlations in Exchange Coupled Systems, Reidel, Dordrecht, 1983, p. 463.
169 D.N. Hendrickson, in R.D. Willett, D. Gatteschi and O. Kahn (Eds.), Magneto-structural Correlations in Exchange Coupled Systems, Reidel, Dordrecht, 1983, p. 525.
170 H.U. Güdel, A. Stebler and A. Furrer, Inorg. Chem., 18 (1979) 1021.
171 F.A. Cotton, B.G. DeBoer, M.D. LaPrade, J.R. Pipal and D.A. Ucko, Acta Crystallogr. Sect. B, 27 (1971) 1664.
172 L. Dubicki, Aust. J. Chem., 25 (1972) 1141.
173 A.E. Hansen and C.J. Ballhausen, Trans. Faraday Soc., 61 (1965) 631.
174 R.D. Willett, J. Chem. Phys., 44 (1966) 39.
175 R.D. Willett and C. Chow, Acta Crystallogr. B, 30 (1974) 207.
176 S.R. Desjardins, D.E. Wilcox, R.L Musselman and E.I. Solomon, Inorg. Chem., 26 (1987) 288.
177 A. Bencini and D. Gatteschi, personal communication to authors of ref. 176.
178 M.K. Johnson, A.E. Robinson and A.J. Thomson, Met. Ions Biol., 4 (1982) 367.
179 H.J. Schugar, G.R. Rossman, C.G. Barraclough and H.B. Gray, J. Am. Chem. Soc., 94 (1972) 2683.

180 H.B. Gray, in R.R. Crighton (Ed.), Proteins of Iron Storage and Transport in Biochemistry and Medicine, North-Holland, Amsterdam, 1975, p. 3.
181 M.V. Hanson, C.B. Smith and G.O. Carlisle, Inorg. Nucl. Chem. Lett., 11 (1975) 865.
182 G.O. Carlisle and G.D. Simpson, J. Mol. Struct., 25 (1975) 219.
183 R.D. Willett, D. Gatteschi and O. Kahn (Eds.), Magneto-structural Correlations in Exchange Coupled Systems, Reidel, Dordrecht, 1983.
184 E.R. Bernstein and G.R. Meredith, J. Chem. Phys., 64 (1976) 375.
185 L. Dubicki, J. Ferguson, E.R. Krausz, P.A. Lay, M. Maeder and H. Taube, J. Phys. Chem., 88 (1984) 3940.
186 G.A. Prinz and E. Cohen, Phys. Rev., 165 (1968) 335.
187 M.J.M. Leask and D. Smith, J. Chem. Phys., 51 (1969) 4305.
188 W. Fricke, Z. Phys., B33 (1979) 255, 261.
189 N. Pelletier-Allard and R. Pelletier, J. Phys. (Paris), 43 (1982) 403.
190 R. Buisson, J. Lumin., 31–32 (1984) 78.
191 R. Buisson and J.C. Vial, J. Phys. (Paris), Lett., 42 (1981) L115.
192 J.C. Vial and R. Buisson, J. Phys. (Paris), Lett., 43 (1982) L339.
193 R.B. Barthem, R. Buisson and J.C. Vial, J. Phys., Colloq., C7 (1985) 483.
194 R.B. Barthem, R. Buisson, J.C. Vial and H. Harmand, J. Lumin., 34 (1986) 295.
195 R.B. Hunt and R.G. Pappalardo, J. Lumin., 34 (1985) 133.
196 F.J. Weesner, J.C. Wright and J.J. Fontanella, Phys. Rev. B, 33 (1986) 1372.
197 S.I. Mho and J.C. Wright, J. Chem. Phys., 79 (1983) 3962.
198 F. Varsanyi and G.H. Dieke, Phys. Rev. Lett., 7 (1961) 442.
199 G.H. Dieke and E. Dorman, Phys. Rev. Lett., 11 (1963) 17.
200 D.L. Dexter, Phys. Rev., 126 (1962) 1962.
201 D.L. Dexter, J. Chem. Phys., 21 (1953) 836.
202 R.W. Schwartz, Inorg. Chem., 16 (1977) 1694.
203 H.J. Schugar, E.I. Solomon, W.L. Cleveland and L. Goodman, J. Am. Chem. Soc., 97 (1975) 6442.
204 R.T. Brundage and W.M. Yen, Phys. Rev. B, 34 (1986) 8810.
205 H.Y. Zhang, R.T. Brundage and W.M. Yen, J. Lumin., 31–32 (1984) 257.
206 R. Buisson, J.Q. Liu and J.C. Vial, J. Phys. (Les Ulis, Fr.), 45 (1984) 1533.
207 B. DiBartolo (Ed.), Energy Transfer Processes in Condensed Matter, Plenum, New York, 1984.
208 R.C. Powell and G. Blasse, Struct. Bonding (Berlin), 42 (1980) 43.
209 W.M. Yen and P.M. Selger (Eds.), Laser Spectroscopy in Solids, Topics in Applied Physics, Vol. 9, Springer, Berlin, 1981.